JOURNAL OF GEOPHYSICAL RESEARCH, VOL. 115, B07308, doi:10.1029/2009JB006882, 2010

Structure of the upper mantle and transition zone beneath Southeast Asia from traveltime tomography

Chang Li[1] and Robert D. van der Hilst[2]

Received 13 August 2009; revised 11 January 2010; accepted 22 January 2010; published 16 July 2010.

[1] Tomographic images of the mantle beneath East Asia were obtained from the inversion of traveltime data from global and regional seismograph networks and from temporary arrays on and around the Tibetan plateau. Our results are consistent with previous studies but the unprecedented resolution of mantle heterogeneity provides new insight into the large-scale tectonic framework of the continental India-Asia collision in the western part of the study region and subduction of the oceanic lithosphere in the east. In the realm of continental collision, west of ~100°E, a relatively slow *P*-wave speed characterizes the upper mantle beneath much of the Tibetan plateau but the wave speed is high beneath cratonic India, the southern and western part of the Tibetan plateau, Hindu-Kush, and the Tian Shan. In the subduction realm, east of ~110°E, the main structures are (i) pronounced low-wave-speed anomalies at a depth of between 100 and 400 km beneath Asia's southeastern seaboard and the back-arc regions of ongoing subduction; (ii) narrow, fast anomalies in the upper mantle beneath major subduction zones; and (iii) widespread fast anomalies at a depth of 500–700 km beneath the Sea of Japan, the northern part of the Philippine Sea plate, and southeastern China. If the latter anomalies represent stagnant slabs, their fragmented nature and large lateral extent suggest that they are produced by different episodes of subduction beneath western Pacific island arcs, along the old SE margin of Asia, or during the Mesozoic collision of cratonic units in Southeast Asia. Attribution to ancient subduction systems implies that slab fragments can reside in the transition zone for (at least) several tens of millions of years. Shallow, slow anomalies beneath the Red River fault region connect to deep anomalies beneath the South China fold belt and South China Sea, suggesting a causal relationship between the evolution of the continental lithosphere of SW China and deeper mantle processes. Between the collision and the subduction realms, tomography reveals high-wave-speed continental roots beneath the western part of the North China craton (Ordos block) and the South China, or Yangtze, craton (Sichuan Basin) to a depth of ~300 km.

Citation: Li, C., and R. D. van der Hilst (2010), Structure of the upper mantle and transition zone beneath Southeast Asia from traveltime tomography, *J. Geophys. Res.*, *115*, B07308, doi:10.1029/2009JB006882.

1. Introduction

[2] The large-scale tectonic evolution of Southeast Asia has been influenced by a long, complex history of subduction of the oceanic lithosphere along its extensive eastern and southeastern margins and by subduction of the Tethys ocean floor below and (since ~55 Ma) collision of the Indian subcontinent with mainland Asia. The large-scale system formed by the northward push in the west and the (south) eastward pull in the (south)east (Figure 1) has produced a diverse range of geological structures—from the Tibetan plateau and the majestic mountain ranges surrounding it in the west to the continental rifts and a plethora of marginal basins and volcanic arcs in the east—and may have facilitated substantial eastward mass transport from the central part of the collision zone to the eastern margins and into Indochina, a key component of the geological evolution of Southeast Asia [e.g., *Molnar and Tapponnier*, 1975; *Tapponnier et al.*, 1982, 2001; *Royden et al.*, 2008]. In addition to these (near-surface) manifestations, there are likely to be causal relationships with structural heterogeneity and geodynamical processes deeper in the Earth. Imaging and understanding these structures and processes is the subject of the research reported here.

[3] There seems little doubt that subduction has produced substantial heterogeneity in the mantle beneath Southeast Asia. The Cenozoic retreat of the western Pacific and Philippine Sea slabs that generated island arcs, marginal seas, and a number of continental rifts and extension zones in northeast China [*Northrup et al.*, 1995; *Schellart et al.*, 2003; *Zhang et al.*, 2003; *Schellart and Lister*, 2005] has

[1]Geoscience Technology, Hess Corporation, Houston, Texas, USA.
[2]Department of Earth, Atmospheric, and Planetary Sciences, Massachusetts Institute of Technology, Cambridge, Massachusetts, USA.

0148-0227/10/2009JB006882

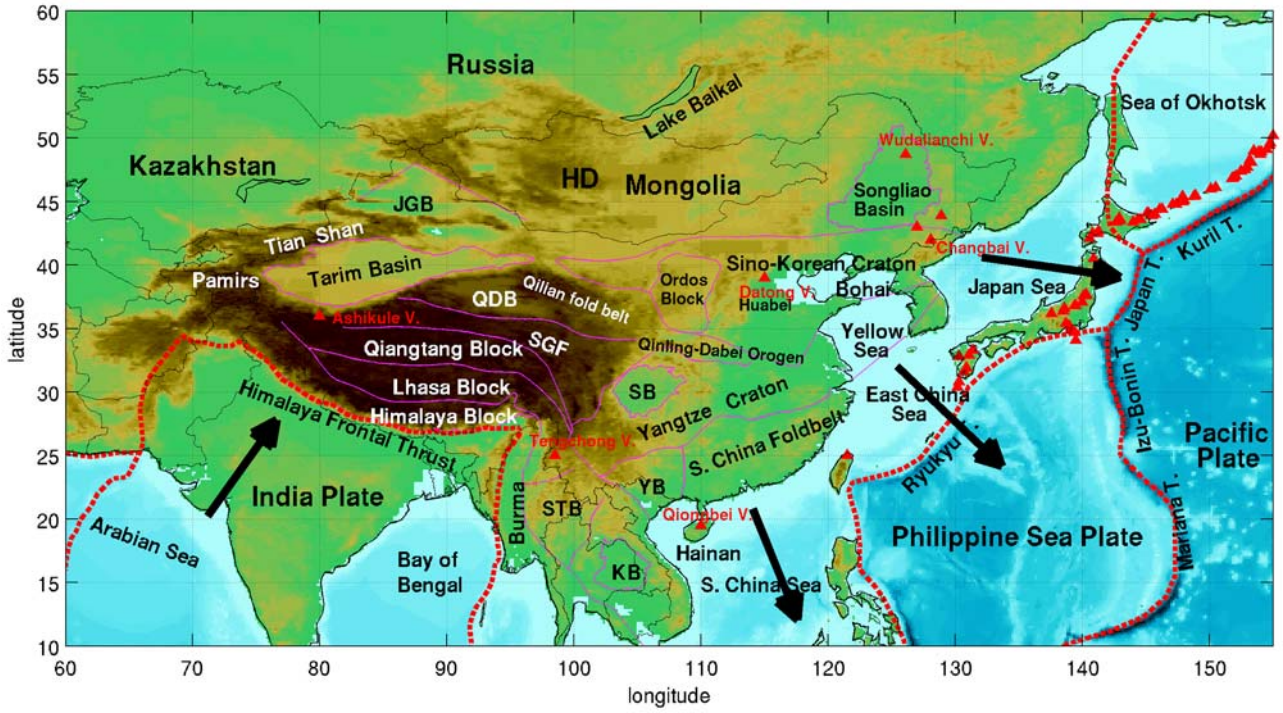

Figure 1. Topographic map of East Asia with the tectonic units that are referred to in the text. Dashed red lines are plate boundaries, according to NUVEL-1 [*DeMets et al.*, 1990]. Thick purple lines denote the main tectonic units: HD, Hangayn Dome; SB, Sichuan basin; KB, Khorat basin; STB, Shan Thai block; YB, Youjiang block; JGB, Junggar basin; SGF, Songpan Ganzi Fold belt. Red triangles represent recently active volcanoes. Black arrows illustrate northward motion of the Indian plate and (south)eastward retreat of the Pacific trench systems.

been linked to the stagnation of subducted slab material in the mantle transition zone inferred from traveltime tomography [*Van der Hilst et al.*, 1991; *Fukao et al.*, 1992, 2001; *Van der Hilst and Seno*, 1993; *Huang and Zhao*, 2006; *Miller et al.*, 2006], and the tomographically inferred higher-than-average wave speeds in the lowermost mantle beneath East Asia may depict structures produced by deep subduction along the eastern seaboard of Asia well before the Eocene onset of oceanward trench migration and concomitant back-arc extension [*Kárason and Van der Hilst*, 2001]. Similarly, the large-scale high-wave-speed anomaly in the mid mantle from beneath the Sunda arc to the Mediterranean has been explained by Mesozoic subduction of the Tethys ocean floor and, later, parts of the Indo-Australian plate along the southern margin of Asia [*Widiyantoro and Van der Hilst*, 1996; *Grand et al.*, 1997; *Van der Hilst et al.*, 1997; *Van der Voo et al.*, 1999; *Replumaz et al.*, 2004; *Hafkenscheid et al.*, 2006].

[4] Vice versa, deep mantle processes may have influenced geological phenomena manifested near the surface. For example, subduction-induced mantle upwelling has been invoked to explain widespread uplift, volcanism, and extension of East China [*Tatsumi et al.*, 1990; *Tian et al.*, 1992; *Yin*, 2000; *Liu et al.*, 2001; *Zhao et al.*, 2004], and slab roll-back may have aided the southward motion of Indochina [*Widiyantoro and Van der Hilst*, 1996]. Either continuously or intermittently, trench migration has occurred along the eastern margin of Asia, from the Kurils in the north to the Philippines in the southeast and Java-Sumatra in the south [*Hall*, 2002; *Honza and Fujioka*, 2004]. Because of the length of this plate boundary system, it is possible that slab roll-back influenced lithosphere and upper mantle deformation as far west as the Baikal rift zone [*Schellart and Lister*, 2005; *Lebedev et al.*, 2006] and that it facilitated large-scale eastward transport of lithospheric material from the realm of continental collision in the west to the realm of subduction in the east and southeast [*Royden et al.*, 2008].

[5] To understand the cause and effect of these large-scale processes, we need to know the three-dimensional (3-D) structure of Earth's mantle. *Lebedev and Nolet* [2003] gave an excellent overview of tomographic studies of mantle heterogeneity beneath East Asia conducted over the past two decades. Surface-wave tomography provides good constraints on the structure of the shallow upper mantle even in regions where station distribution is relatively sparse. In Southeast Asia it has revealed Precambrian continental roots ~300 km thick beneath the Sichuan basin and the Ordos block [*Lebedev and Nolet*, 2003] and fast shear-wave propagation beneath western and southern Tibet in some models [*Romanowicz et al.*, 1982; *Wu et al.*, 1997; *Friederich*, 2003; *Lebedev and Van der Hilst*, 2008] and under much of the plateau in others [*Griot et al.*, 1998; *Shapiro and Ritzwoller*, 2002; *Priestley et al.*, 2006]. With higher mode data, *Lebedev and Nolet* [2003] detected seismically fast anomalies in the transition zone beneath the South China (Yangtze) craton. However, the horizontal resolution of traditional surface-wave tomography is

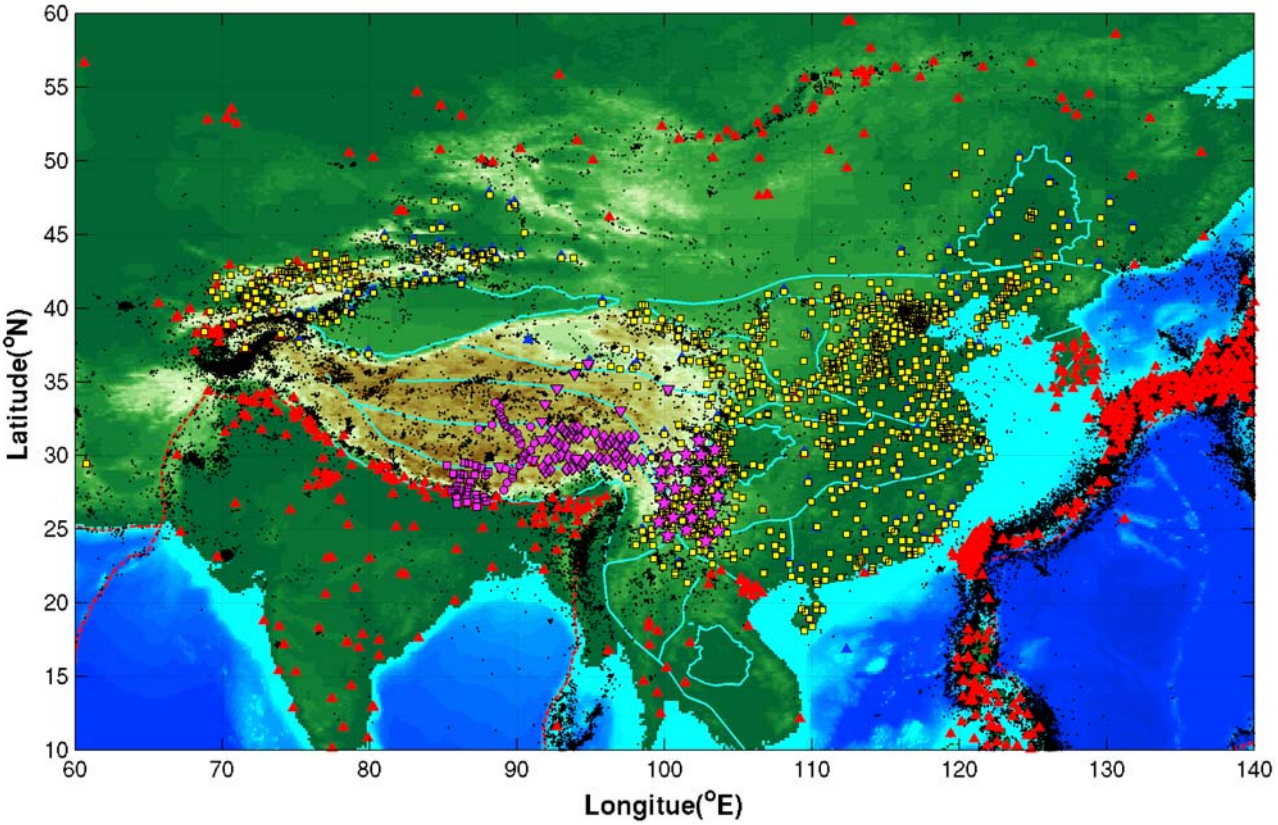

Figure 2. Distribution of regional stations and earthquakes (black dots) that contributed travel time data used in inversions. Red triangles depict ~1300 stations of the EHB [*Engdahl, van der Hilst, and Buland* 1998] in East Asia; yellow squares are ~1000 stations in the Chinese Seismograph Network; and magenta samples represent stations of seismic arrays in the Tibetan plateau. From east to west: stars, MIT-CIGMR array (2003–2004); diamonds, Lehigh-CIGMR array (2003–2004); inverse triangles, Sino-American array (1991–1993); dots, International Deep Profiling of Tibet and the Himalaya (INDEPTH)-II (1994) and INDEPTH-III (1998–1999); squares, Himalayan Nepal Tibet array (2001–2003).

generally no better than 500 km because of the relatively low-frequency data used. Moreover, surface-wave data gradually lose resolution with increasing depth, in particular, when the analysis is restricted to fundamental-mode surface-wave propagation. With continuous data from dense regional arrays, ambient noise (surface)-wave tomography provides high-resolution images [*Shapiro et al.*, 2005; *Yao et al.*, 2006, 2008], but this concerns relatively short periods and is, therefore, best used for crustal studies.

[6] Traveltime tomography can resolve the deep mantle structure better than surface-wave tomography, and in geographic areas with good data coverage it also provides better lateral resolution of the shallow mantle structure (albeit often with worse resolution in the radial direction). Two decades ago tomography with *P*-wave data from the International Seismological Centre revealed the presence of stagnant slabs in the mantle transition zone beneath the Japan Sea, the northern part of the Philippine Sea, and East China, with slabs penetrating to larger depths beneath other parts of the arc system [e.g., *Zhou and Clayton*, 1990; *Van der Hilst et al.*, 1991, 1993; *Fukao et al.*, 1992, 2001]. With data from Chinese seismograph networks becoming more openly available, combinations of data from global networks and from stations in China have been used to confirm and study in more detail the stagnant slabs in the mantle transition zone beneath Southeast Asia [e.g., *Huang and Zhao*, 2006], but their lateral extent and continuity, which are important for interpretation, have not yet been established.

[7] We present results of tomographic inversion of traveltime data from global bulletins, from ~1000 stations in the Chinese provincial networks, and from ~170 stations from seismic arrays in SW China and Tibet (Figure 2). Many previous tomographic studies have focused on the mantle structure beneath northwestern Pacific island arcs, Indochina, or the central collision zone; here we focus on mantle heterogeneity beneath the mainland of East Asia. Our new images are generally consistent with previous results but shed new light on our understanding of the large-scale tectonics in the region and the influence of plate boundary dynamics. In particular, the images suggest that the "graveyard" of stagnant slabs in the mantle transition zone is more widespread and fragmented than previously thought and may have been produced by multiple subduction systems.

2. Data and Methods

[8] For a detailed description of the data and methods used for our tomographic inversions, we refer to *Li et al.*

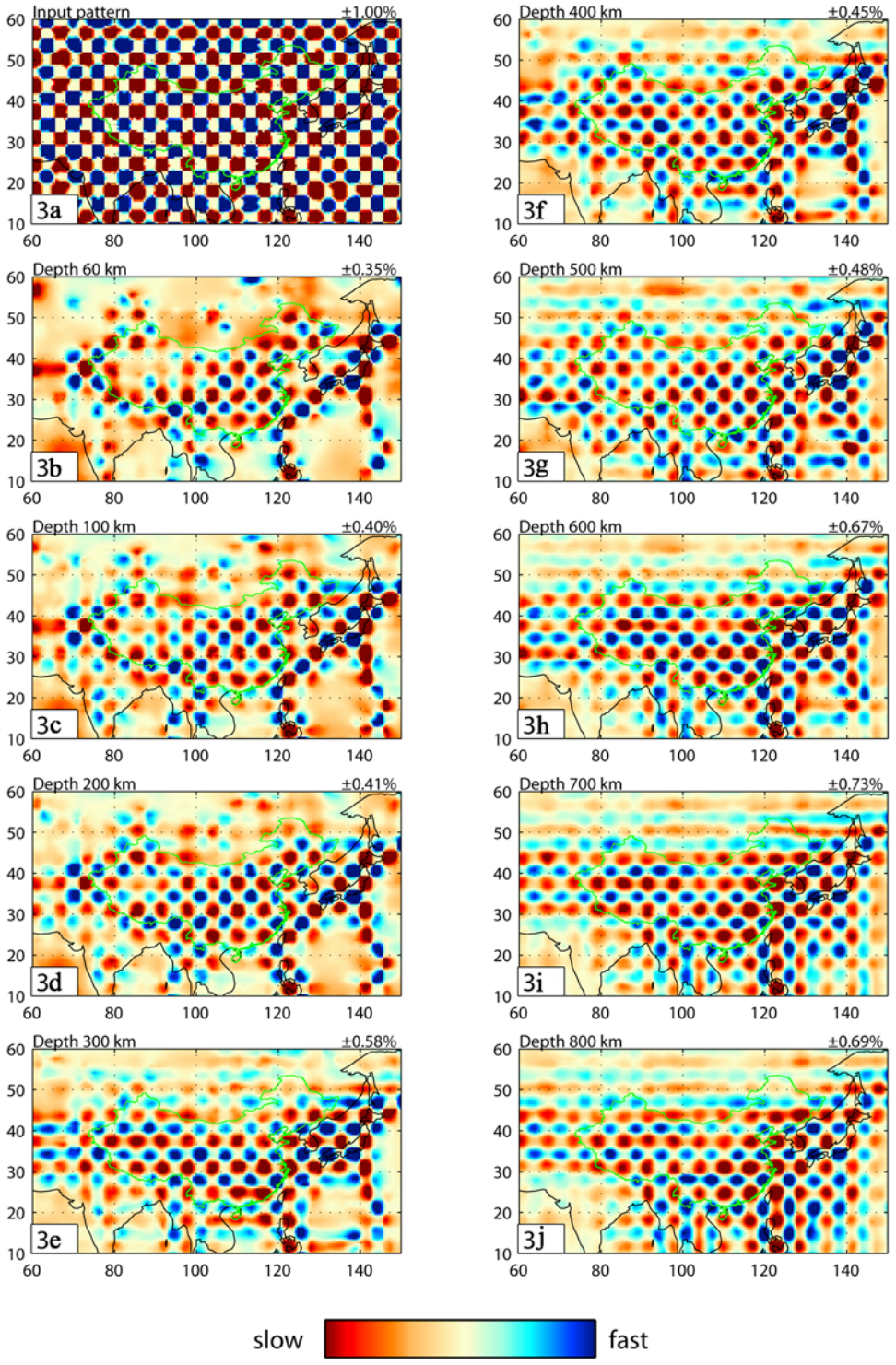

Figure 3. Checkerboard resolution test for target anomalies at different depths. (a) Input pattern: 3° × 3° in horizontal size, with a ±1.0% velocity variation. The amplitude range of the output model is given above the top right corner of each plot. The green line is the boundary of China and the black line represents coastline.

[2008a, 2008b]. The traveltimes most relevant for this study are obtained from three sources. First, from *Li et al.* [2008b], we used ~35,000 *P*-wave phase arrivals picked from records at ~170 stations of seismograph arrays deployed on or near the plateau (Figure 2; magenta symbols). Second, we used more than 1 million *P* picks from earthquakes between 1967 and 2004 recorded at one or more of ~1000 stations in the Chinese Seismograph Network (Figure 2; yellow squares). This includes but far exceeds the data from the Annual Bulletin of Chinese Earthquakes used by *Li et al.* [2006] and

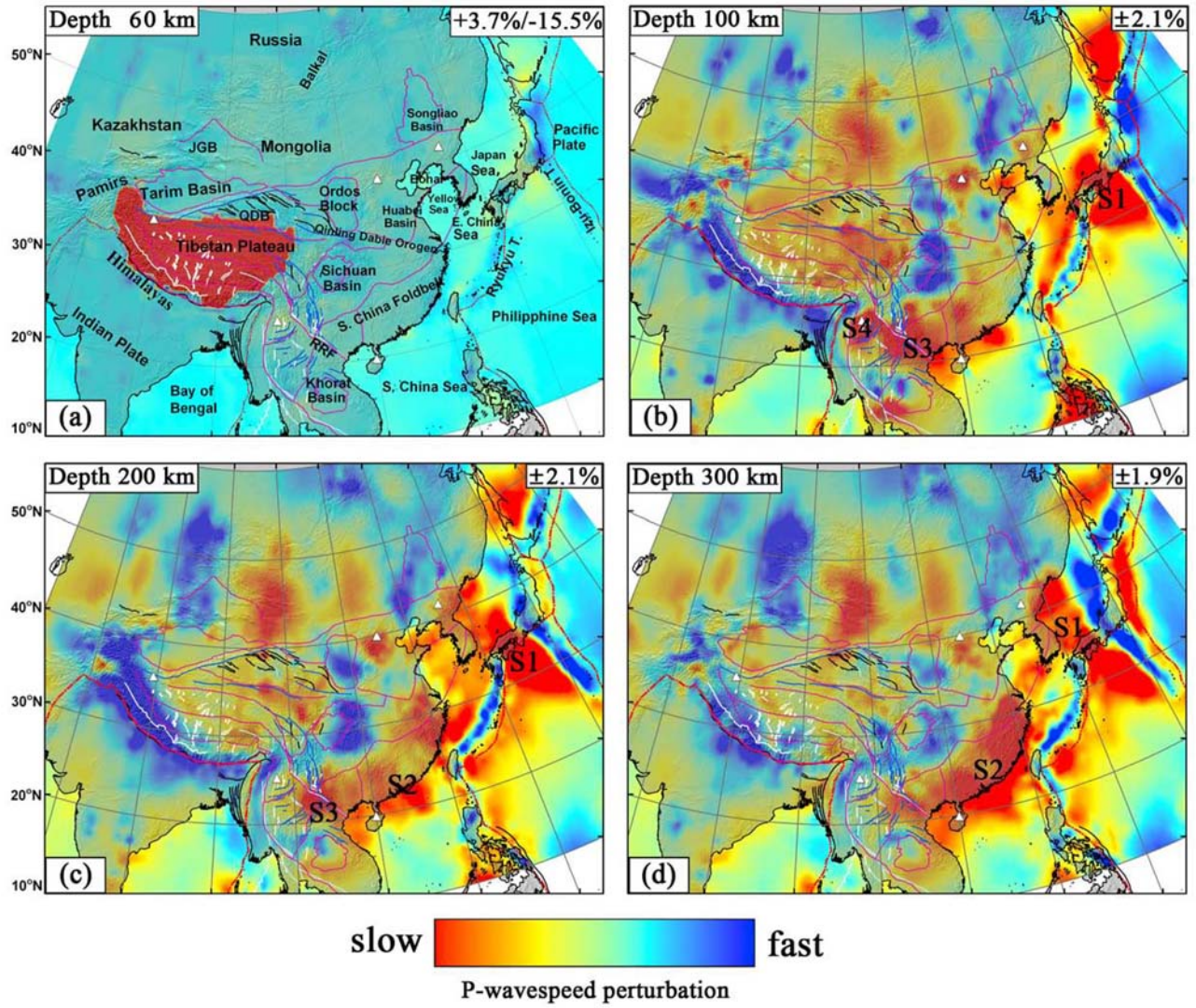

Figure 4. Lateral variation in *P*-wave speed, relative to the *ak135* [*Kennett et al.*, 1995] reference model, at different depths beneath Southeast Asia. Blue and red represent fast and slow perturbation, respectively. The depth of each layer is given in the top left corner, and the magnitude range is given in the top right corner, of each plot. White triangles depict recently active volcanoes in mainland China. The coastlines (black), tectonic block boundary (pink), and plate boundary (dashed red) are the same as in Figure 1. The main fault systems in and around the Tibetan plateau (white, norm faults; blue, strike-slip faults; black, thrust faults) are shown. (b–e) Upper mantle structures S1, S2, S3, and S4 and (f, g) transition-zone structures TZ1 (TZ1A and TZ1B), TZ2, and TZ3 (TZ3A and TZ3B) are discussed in the text.

Huang and Zhao [2006]. Third, we use ~12 million *P*, *Pg*, *pP*, *Pn*, and *PKP* phases (1964–2007) from International Seismological Centre data processed by *Engdahl et al.* [1998], hereinafter referred to as EHB data (Figure 2; red triangles). To avoid overlap, internal inconsistency, and differences in baseline, upon merging these data sets, Engdahl and Bergman (personal communication) remove duplicate time reports, fix problems with conflicting station codes or inaccurate (or incorrect) station coordinates, and subject all data and events to a nonlinear process of earthquake relocation and phase reidentification [as in *Engdahl et al.*, 1998] using the *ak135* traveltime tables [*Kennett et al.*, 1995].

[9] These short-period data are inverted along with a global data set of ~22,000 differential traveltime residuals of *PP-P*, which helps constrain the upper mantle structure beneath regions with few earthquakes and stations. We use 3-D approximated sensitivity kernels to account for the finite frequency effect of low-frequency *PP-P* differential data [*Kárason and Van der Hilst*, 2001; *Kárason*, 2002], an adaptive grid parameterization, and a crust correction [*Li et al.*, 2006] to account for effects of crustal heterogeneity (e.g., beneath Tibet) that cannot be resolved well with the data used. The tomographic system of equations is solved using the LSQR algorithm [*Paige and Saunders*, 1982; *Nolet*, 1985].

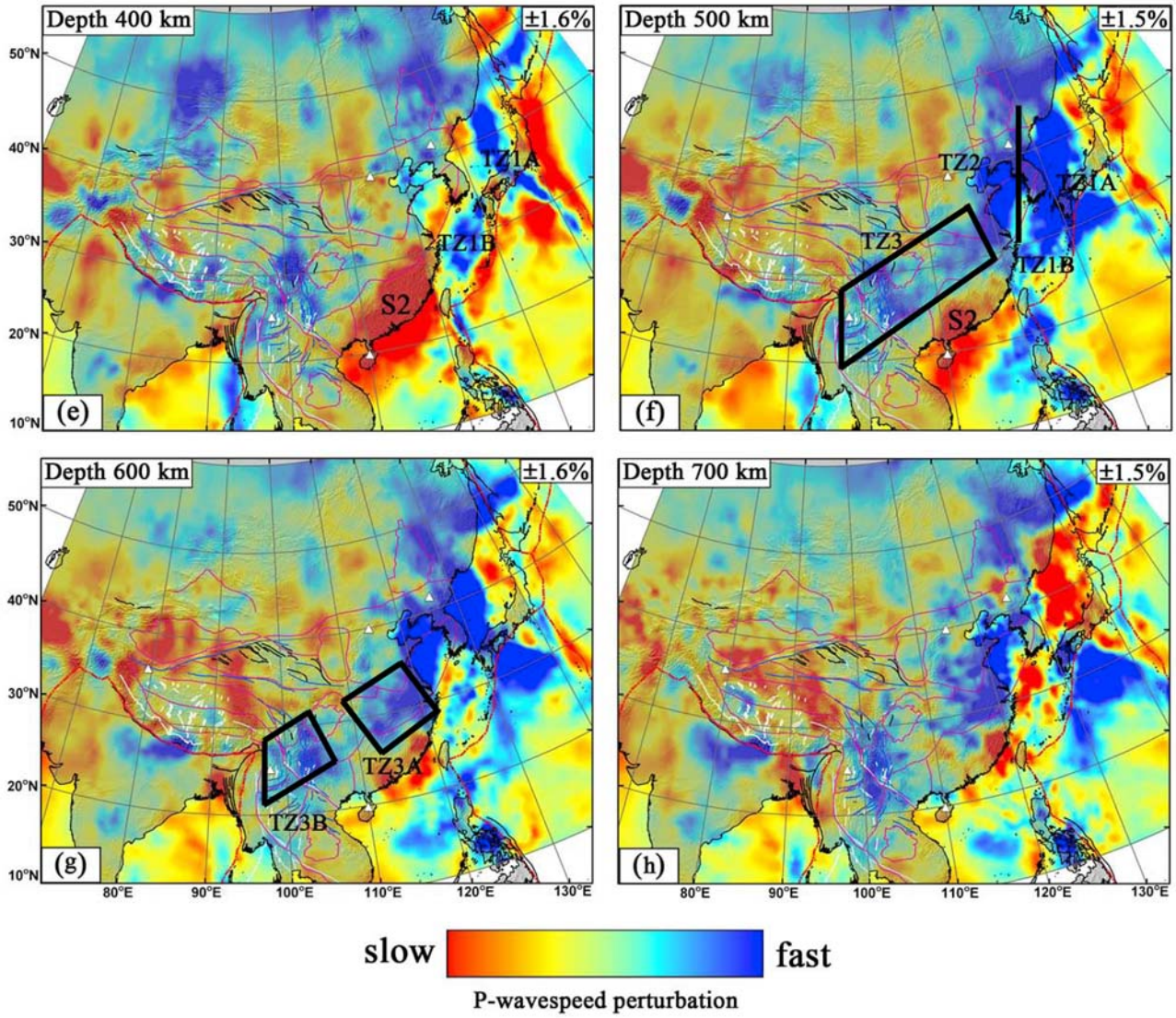

Figure 4. (continued)

[10] To assess the performance of the inversion algorithm and obtain a qualitative impression of the resolution by the data, we have conducted tests with traveltime data calculated from known input structures. Checkerboard tests have limited diagnostic value [e.g., *Van der Hilst et al.*, 1993] but provide a qualitative measure of the performance of tomography for a given data distribution. Figure 3 displays the results of a test used to evaluate the resolution of heterogeneity with a horizontal scale length of the order of 300 km. For this purpose, data computed from a test structure (Figure 3a), inserted at one depth at a time so that "smearing" in the radial direction can be evaluated better, were inverted with the same code and source-receiver distribution as for the inversion of recorded data. As expected, the combination of data used here resolves the input structure better than the data used by *Li et al.* [2006], in particular, in the shallow mantle beneath mainland China and the Tibetan plateau (Figures 3a and 3b). The shallow structure beneath western Tibet and the Tarim basin is not well resolved (Figure 3a), but below ~100 km the depth resolution is adequate under most of the study region (Figures 3d–3h). Resolution tests performed to evaluate specific aspects of the solution are discussed next.

3. Results

[11] We present the tomographically inferred 3-D variations in *P*-wave speed by means of map views at different depths (Figure 4) and vertical mantle profiles (along section lines shown in Figure 5) from the Earth's surface to a depth of about 1700 km (Figure 6).

3.1. Upper Mantle Structure Beneath the Eastern Margin of Eurasia

[12] The most conspicuous features in the images of the eastern margin of Eurasia are the high-velocity anomalies associated with the subducting Western Pacific and Philippine Sea slabs and the low-velocity anomalies beneath

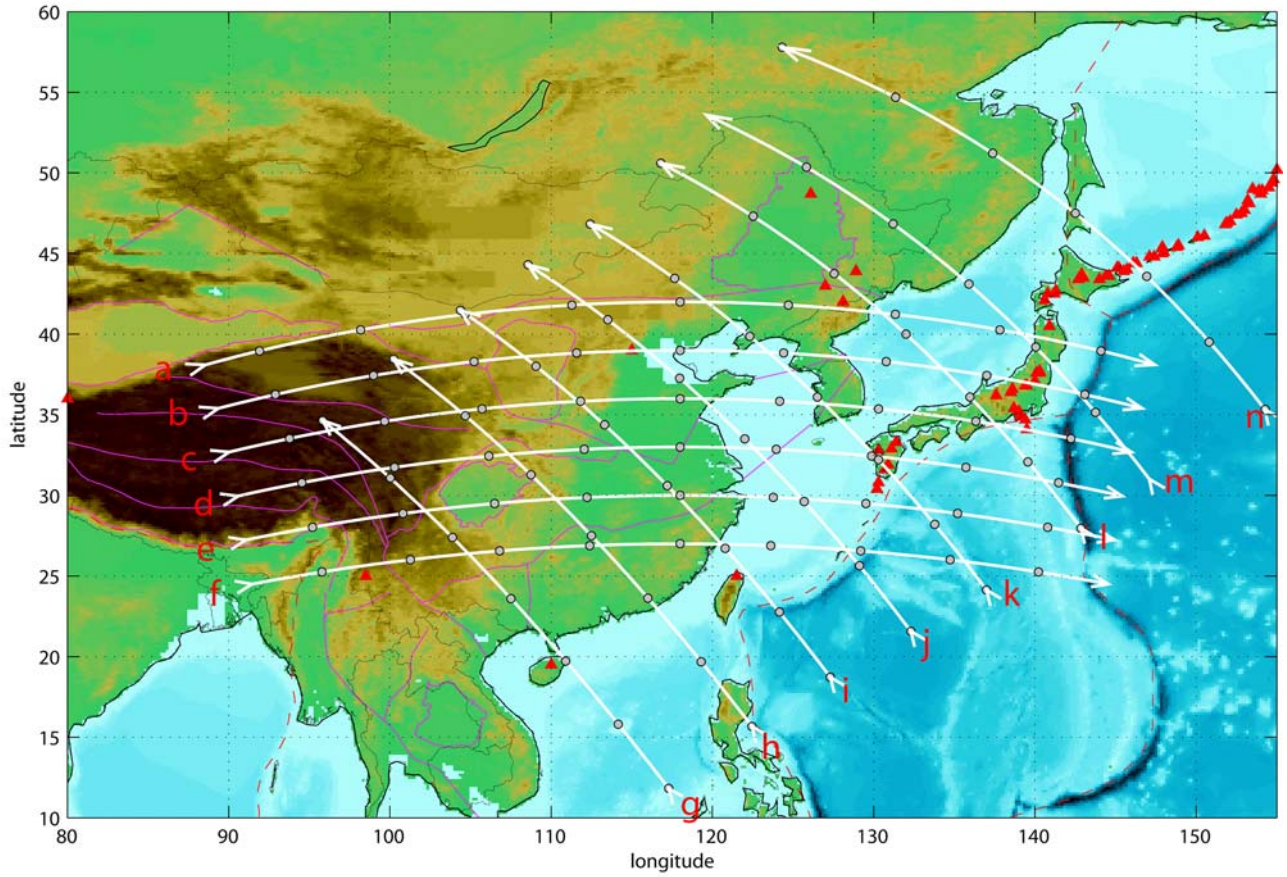

Figure 5. Location of the 14 lines of cross section for which vertical profiles are shown in Figure 6.

the associated back-arc regions. From a 100 to 400 km depth in the mantle, narrow, seismically fast seismogenic structures are clearly visible beneath the Japan and Izu-Bonin trenches (Figures 4a–4e, 6a–6e, and 6l–6n). Another narrow structure, which parallels the Ryukyu trench, is detected beneath the East China Sea (Figures 4b–4e, 6d–6f, and 6i–6k). These structures have been studied extensively since the late 1980s [*Spakman et al.*, 1989; *Zhou and Clayton*, 1990; *Van der Hilst et al.*, 1991; *Fukao et al.*, 1992], and even though the data used here resolve these slabs better, we do not discuss this part of our model in any detail.

[13] The images show widespread low-velocity anomalies in the upper mantle beneath East Asia (e.g., structures S1, S2, S3, and S4 in Figures 4b–4e). Structure S1 (Figures 4b–4e, 6a–6e, and 6l) stretches southeastward from beneath the southern part of the sea, across the shallow mantle beneath the Nankai trough (southwest Honshu, Japan) to the mantle wedges below the Izu Bonin arc. The low wave speeds associated with this back-arc system persist to a depth of ~400 km (Figures 4e, 6a–6e, and 6l), with the strongest anomalies (~2% slower than the *ak135* reference value) occurring under the Izu Bonin island arc. Structure S2 (Figures 4c–4f, 6e, 6f, 6h, and 6i) is located beneath the southeastern margin of mainland China (the South China Fold belt) and the adjacent offshore region in the South China Sea. The northern part of this structure is perhaps associated with back-arc processes of subduction along the Ryukyu arc (Figures 6d–6f), but for the southern part, association with (ongoing or recent) subduction is less obvious. In the transition zone, near ~500 km deep (Figure 4f), S2 seems to be confined to a relatively small region beneath Hainan island and the northern part of the South China Sea. This is qualitatively consistent with the regional study by *Lebedev and Nolet* [2003], but our data do not provide evidence of a deep "plume."

[14] At smaller scales low *P*-wave speed anomalies mark the shallow mantle beneath south China, for example, to a depth of ~200 km beneath the Red River fault zone (S3; Figures 4b, 4c, and 6f). At a greater depth S3 seems to merge with structure S2 (Figures 4c–4f, 6f, and 6g). To the northwest of this area, structure S4 is located near 100 km deep beneath the Tengchong volcanic area (Figures 4b and 6f) and is, most likely, related to subduction below the Burmese arc [*Li et al.*, 2008b].

3.2. Upper Mantle Structure Beneath Basins and Cratons

[15] The data resolve fast *P*-wave propagation beneath most basins and cratonic units in China, such as the Songliao, Ordos, Huabei, Sichuan, and Khorat basins (Figures 4b–4d), and our tomographic images confirm the heterogeneous nature of the present-day North China craton (NCC) and South China (or Yangtze) craton.

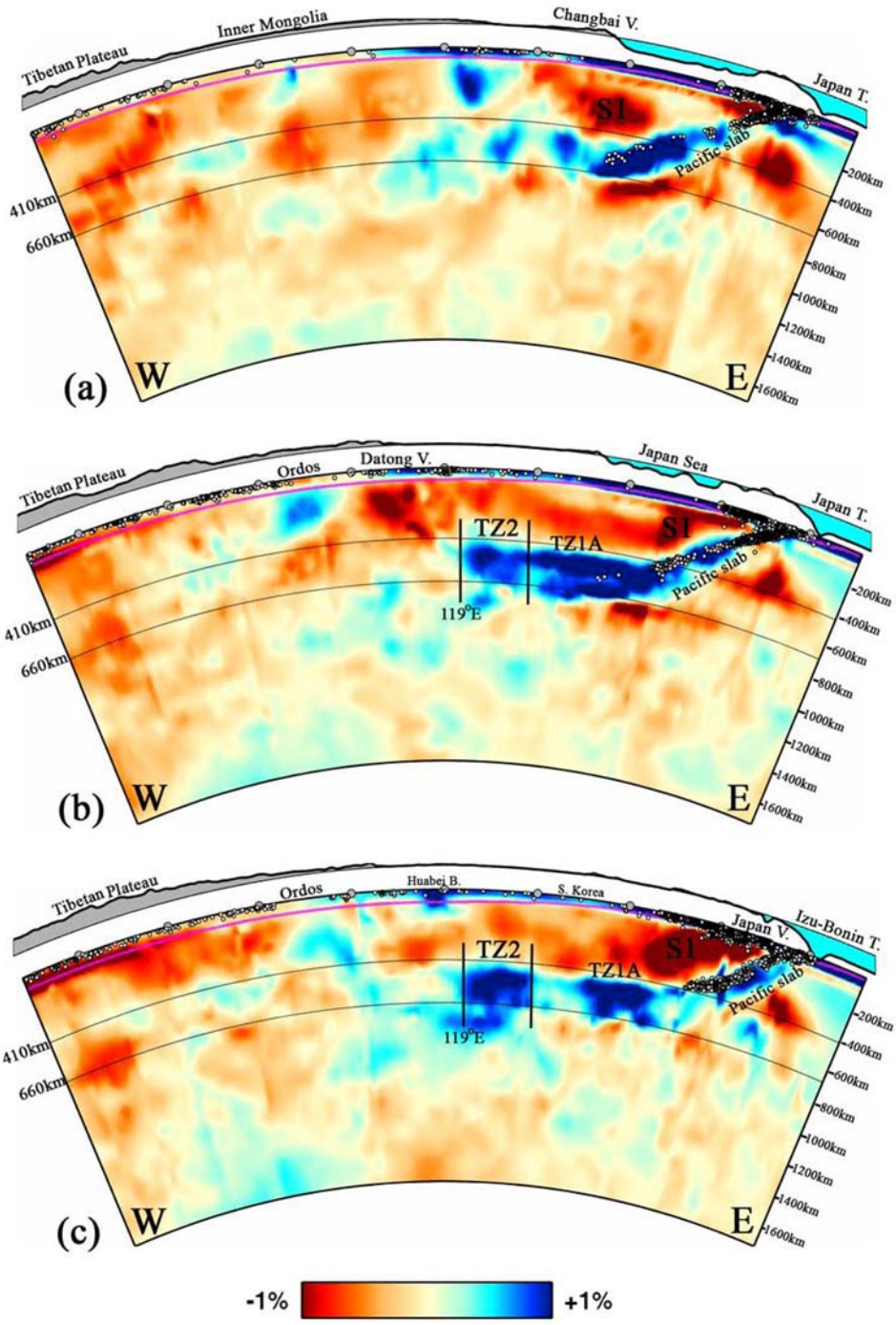

Figure 6. Vertical mantle profiles (along lines of section given in Figure 5) from the Earth's surface to a depth of ~1700 km. For reference, dashed lines at 410 and 660 km depict the position of the discontinuities that define the mantle transition zone. White dots depict the seismic Wadati-Benioff zones of the subducting slabs, and topography is depicted atop the tomographic sections.

[16] Analyses of *Pn* data [*Hearn et al.*, 2004; *Liang et al.*, 2004] indicate fast *P*-wave propagation in the shallow mantle beneath the Ordos and Sichuan basins, which represent the (remaining) Precambrian nuclei of, respectively, the North and South China cratons, and multimode surface-wave tomography has revealed that these basins are underlain by thick (and presumably mechanically rigid) roots of high *S*-wave speed [*Lebedev and Nolet*, 2003]. *Huang and Zhao* [2006] detected fast *P*-wave propagation in the upper mantle beneath these geological units, but the larger data set used here improves the constraints on the 3-D structure of the roots and reveals low wave speeds beneath the Qinling-Dabie orogen between the Ordos and the Yangtze cratons (Figures 7d and 7e).

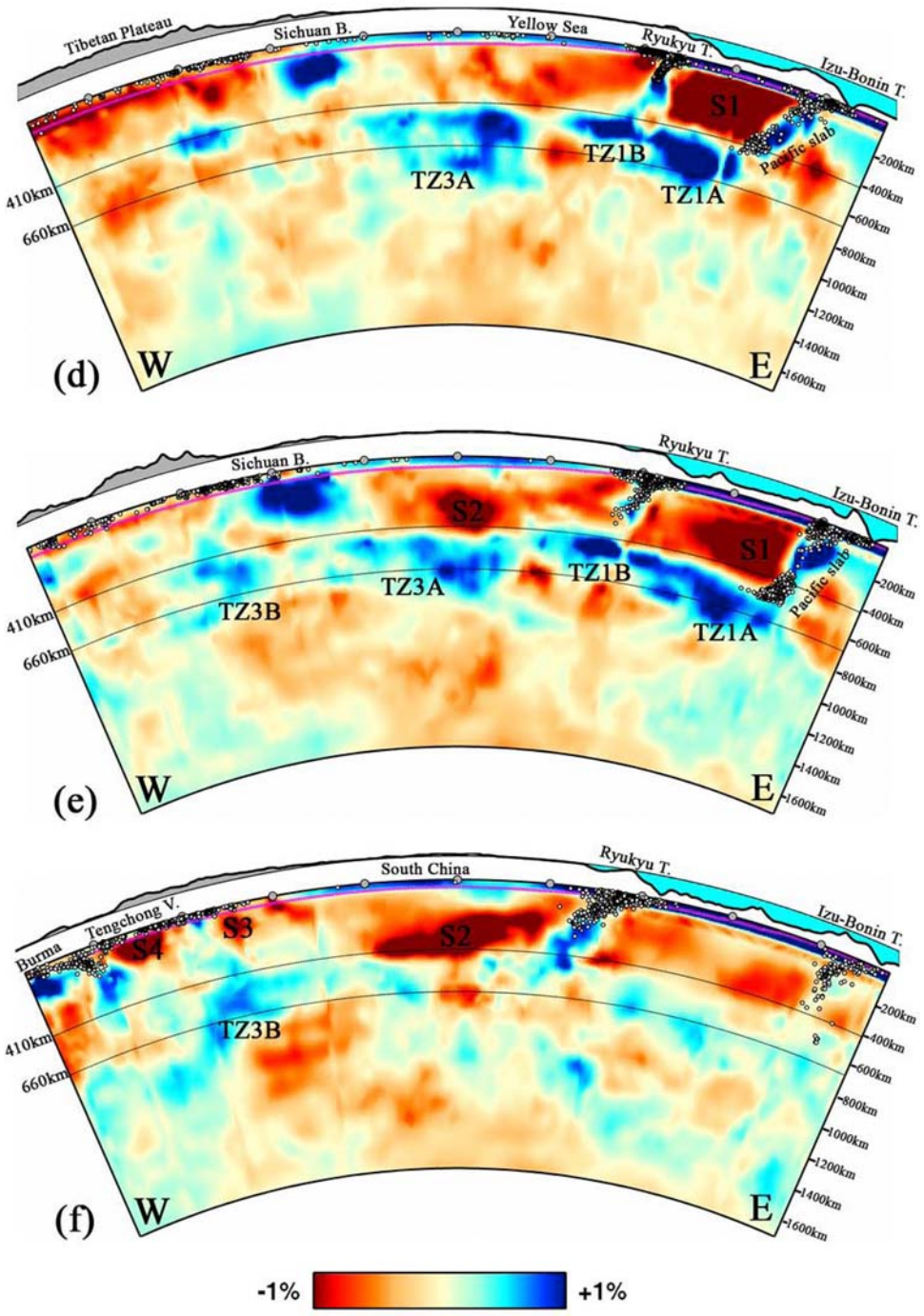

Figure 6. (continued)

[17] The Ordos block is characterized by high-velocity anomalies in the upper mantle to a depth of ~300 km (Figure 7; also Figures 4a–4d, 6b, and 6i). With increasing depth, however, the high-wave-speed anomaly appears to shift southward, and slow propagation speeds appear below the northern part (Figures 4c, 4d, 6b, 6i, and 7e). This heterogeneity within Ordos is in agreement with results from receiver function migration [*Chen et al.*, 2009] and regional surface-wave tomography [*Huang et al.*, 2009]. The Huabei basin (eastern part of the NCC) is marked by fast-wave propagation at shallow depths but does not have a seismically fast root much deeper than ~100 km (Figures 4b and 6c). Wave speeds are slow in the lithospheric mantle beneath the Golf of Bohai and the Changbai volcanic region.

[18] The western part of the Yangtze craton, in particular, the Sichuan basin, is seismically fast to a depth of ~300 km

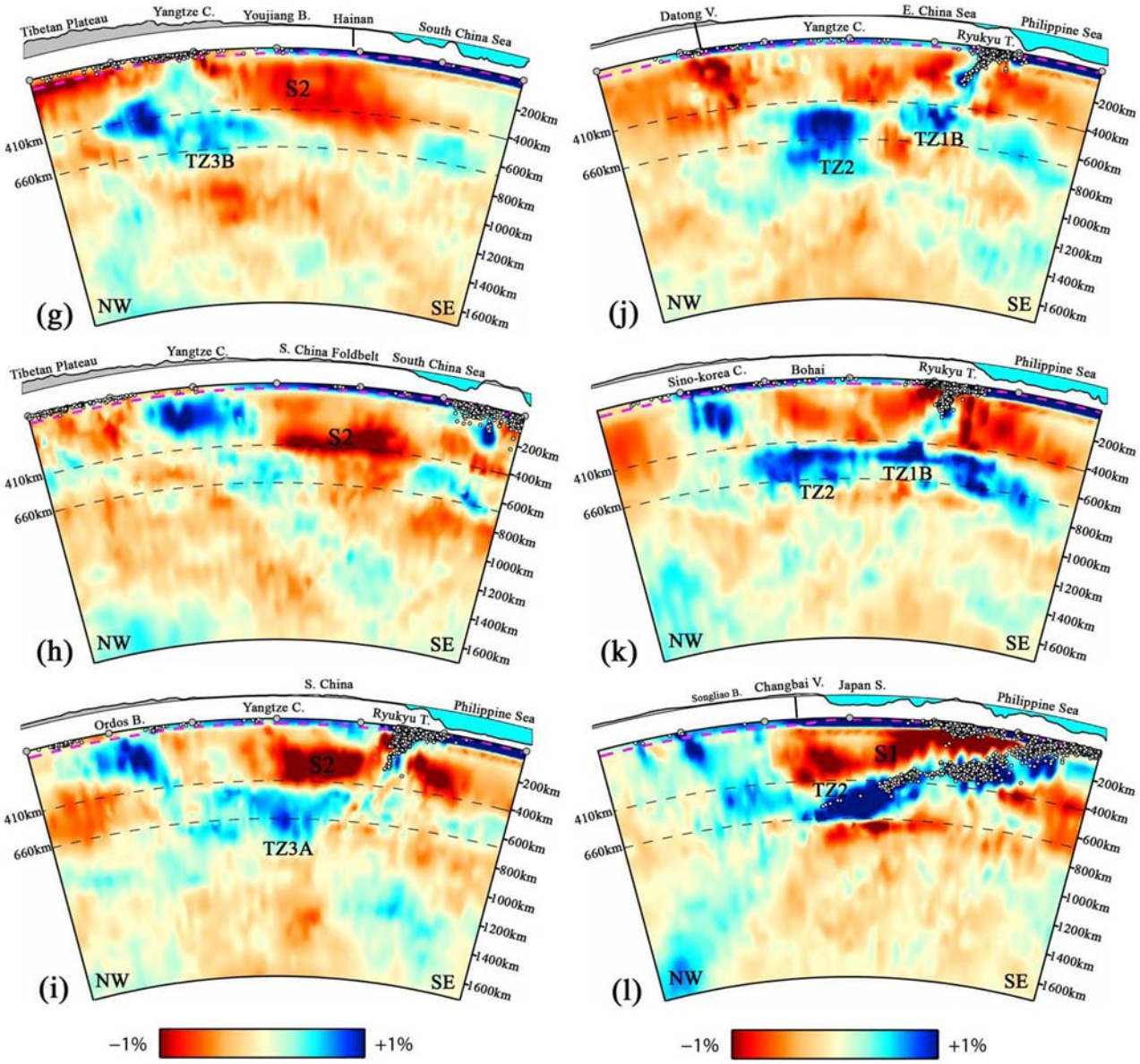

Figure 6. (continued)

(Figures 6d, 6e, and 7). The deeper part of the lithospheric root of the Sichuan basin appears larger than its surface expression and the associated fast anomaly extends eastward to the middle of the Yangtze craton (~112°E; Figure 7), where it forms the western boundary of the widespread low wave speeds beneath the South China fold belt (Figure 6e). Much like Ordos, the root of the Sichuan basin seems to be heterogeneous, with slow *P*-wave propagation beneath its western part and fast-wave propagation beneath the central and the eastern parts (Figure 7). Inversions with synthetic data demonstrate that the vertical and lateral extent of the fast root beneath the western Yangtze craton can be resolved by the data used.

[19] Wave speeds are high beneath the Qaidam basin, but neither it nor the larger Tarim basin is marked by significantly fast anomalies. In fact, *P*-wave speed is rather low in the upper mantle beneath the central and eastern parts of Tarim. This is consistent with the low Rayleigh wave-group velocities observed by *Wu et al.* [1997], but in this region the mantle structure to ~100 km deep is poorly resolved by our data (Figures 3a and 3b).

3.3. Upper Mantle Structure Beneath the Tibetan Plateau

[20] *Li et al.* [2008b] describe mantle heterogeneity beneath the Tibetan plateau and discuss the implications for our understanding of subduction of the Indian lithosphere beneath it. For the sake of completeness, we mention here the most important observations. High wave speeds are detected around the plateau, which is in excellent agreement with results from multimode surface-wave tomography [e.g., *Lebedev and Van der Hilst*, 2008]. Beneath the plateau, however, *P*-wave speed is relatively slow in the shallow mantle. To a depth of ~80 km (e.g., Figure 4a), this simply

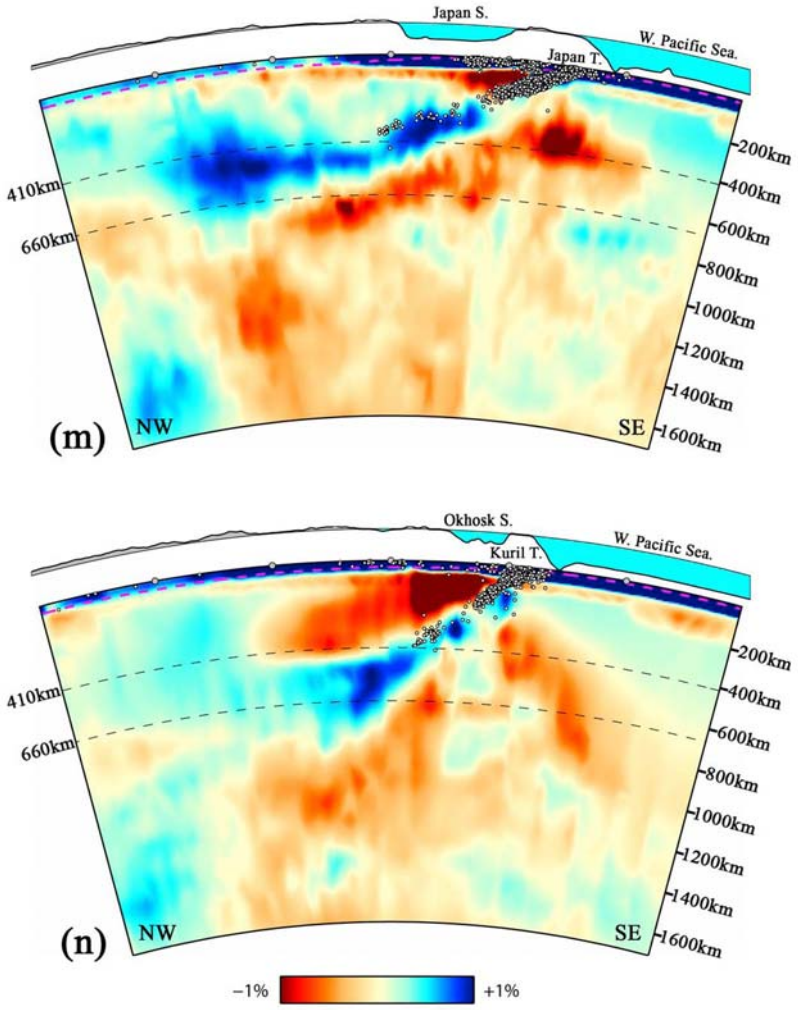

Figure 6. (continued)

reflects the thick crust, but despite the use of crust corrections [*Li et al.*, 2006], the wave speed in the upper mantle beneath the central and eastern plateau appears lower than that beneath the southern and western portion of the plateau and the Hindu-Kush and Tian Shan (Figures 4b–4d).

3.4. Upper Mantle North of the Tibetan Plateau

[21] The data reveal substantial lateral variations in wave speed associated with large cratons and rift systems north of the Tibetan plateau. We mention here the strongest anomalies, but because they are not well resolved by the data used here (Figure 3), we do not discuss them in detail. Strong lateral variations in wave speed are imaged beneath the Juggar basin, from slow-wave propagation in the east to fast in the west (Figures 4b–4d). It is likely that a gradient in elastic properties exists, but in view of the strong lateral variation in image quality (Figures 3a–3c), the images may not represent an accurate depiction of the real structural heterogeneity. East of the Juggar basin and north of the Altyn Tach fault zone a pronounced low-wave-speed anomaly appears in the upper mantle beneath what is known as the "Hangayn Dome" in Mongolia; in our current images this anomaly extends to a depth of at least 300 km (Figures 4b–4d), which may suggest that the Hangayn-Gobi-Altay rift system [e.g., *Barruol et al.*, 2008, and references therein] has a deep origin. We note, however, that vertical resolution is rather poor in this region, and it is likely that *P*-wave traveltime tomography overestimates the depth of the slow anomaly beneath the Hangayn Dome. West of the Hangayn anomaly the images reveal a north-south-trending anomaly of higher-than-average *P*-wave speed, the southern (<50°N) part of which seems to be well resolved in the upper mantle (Figures 3b–3f). This anomaly may represent the western Siberia-Kazakh craton and, perhaps, fossil subduction zones associated with the Variscan Uralide orogeny [*Zonenshain et al.*, 1984; *Matte*, 1995].

3.5. Transition Zone Beneath Southeast Asia

[22] In map view the position of the narrow, seismically fast structures in the upper mantle beneath island arcs, described in section 3.1, shifts westward with increasing depth, which is to be expected if they depict westward-dipping slabs of subducted lithosphere. However, their horizontal width increases dramatically in the mantle transition zone beneath the Japan Sea and East China Sea. These subhorizontal transition zone structures extend over a larger

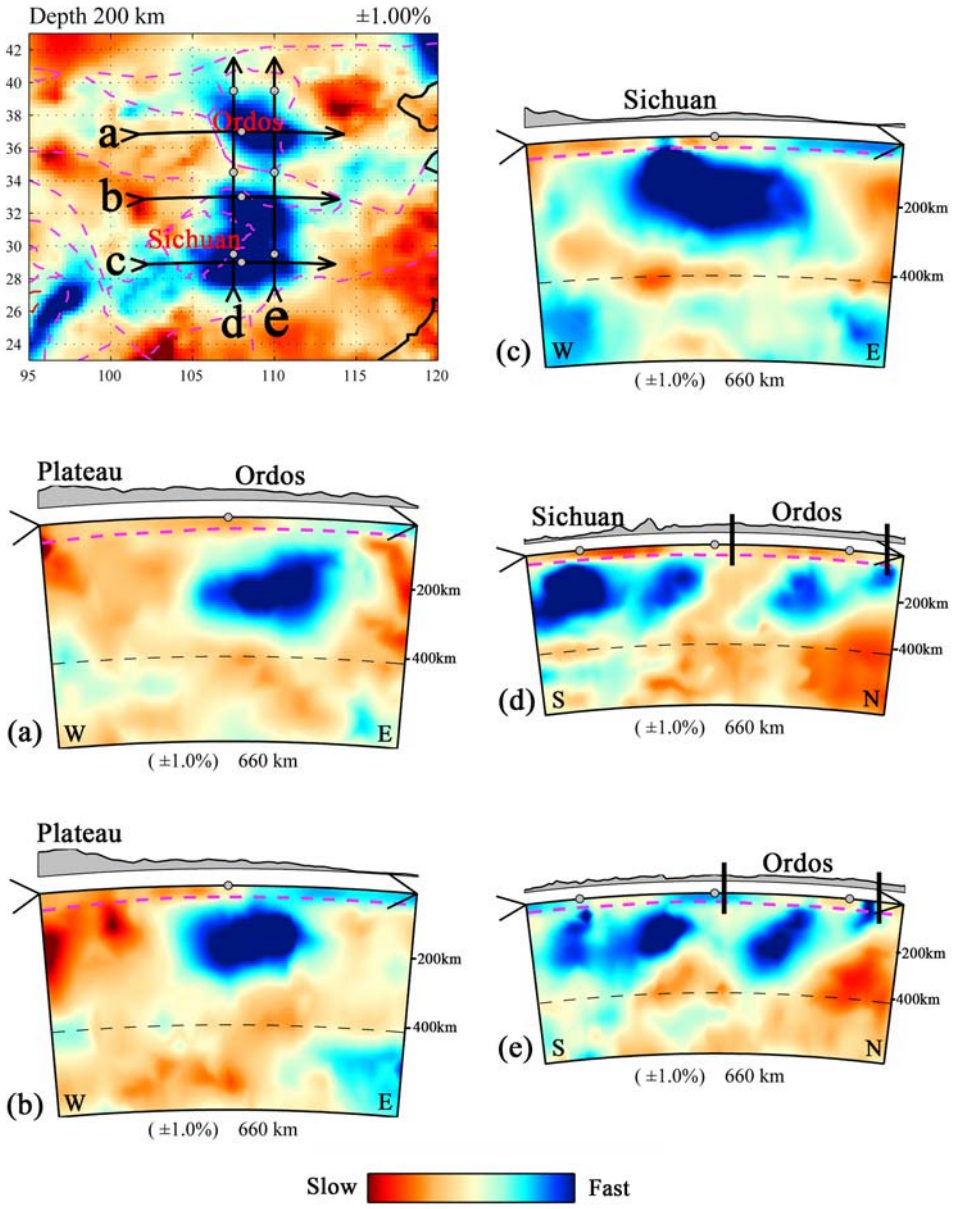

Figure 7. Upper mantle structure beneath the Ordos block and Sichuan basin. (a) Lateral variations in *P*-wave speed at a depth of 200 km. (b–e) Vertical sections to ~600 km depth. Section locations shown in Figure 7a.

region (in particular, toward the west) than inferred from earlier traveltime tomography [e.g., *Van der Hilst et al.*, 1991, 1993; *Fukao et al.*, 1992, 2001; *Huang and Zhao*, 2006; *Miller et al.*, 2006], and their structure appears to be more complicated than could be inferred from the (multimode) surface-wave tomography by *Lebedev and Nolet* [2003].

[23] The tomographic images (Figures 4 and 6) suggest that, instead of a single structure, several separated structures exist in the mantle transition: TZ1 is located beneath the Japan Sea and is parallel to the Japan and Izu-Bonin trenches (TZ1 A) and beneath the Ruykyu arc (TZ1B); TZ2 is a NNE-striking structure beneath the Bohai and the Yellow Sea; and TZ3 is a NE-striking structure beneath the Yangtze Craton and can be further divided into western and eastern parts (TZ3 A and TZ3 B). In the north, structures TZ1 and TZ2 merge and form, in map view, a single structure near 40°N (Figures 6b, 6k, and 6l), but farther south they are clearly separated (Figures 4f, 4g, 6c, and 6j). TZ2 (Figures 4f, 6b, 6c, and 6j–6l) is visible as far west as ~120°E longitude and structure TZ3 extends as far west as ~100°E. We note that the subhorizontal high-wave-speed anomalies are not confined to the transition zone (that is, 410–660 km depth) everywhere; in some regions structures TZ2 and TZ3 A extend to a depth of 800 or even 1000 km (e.g., Figures 6b–6e and 6j).

[24] Beneath the Yangtze craton the transition zone is generally fast (structure TZ3 in Figures 4f, 4g, 6d–6g, and 6i), but upon closer inspection we can distinguish two anomalies (referred to as structures TZ3A and TZ3B in

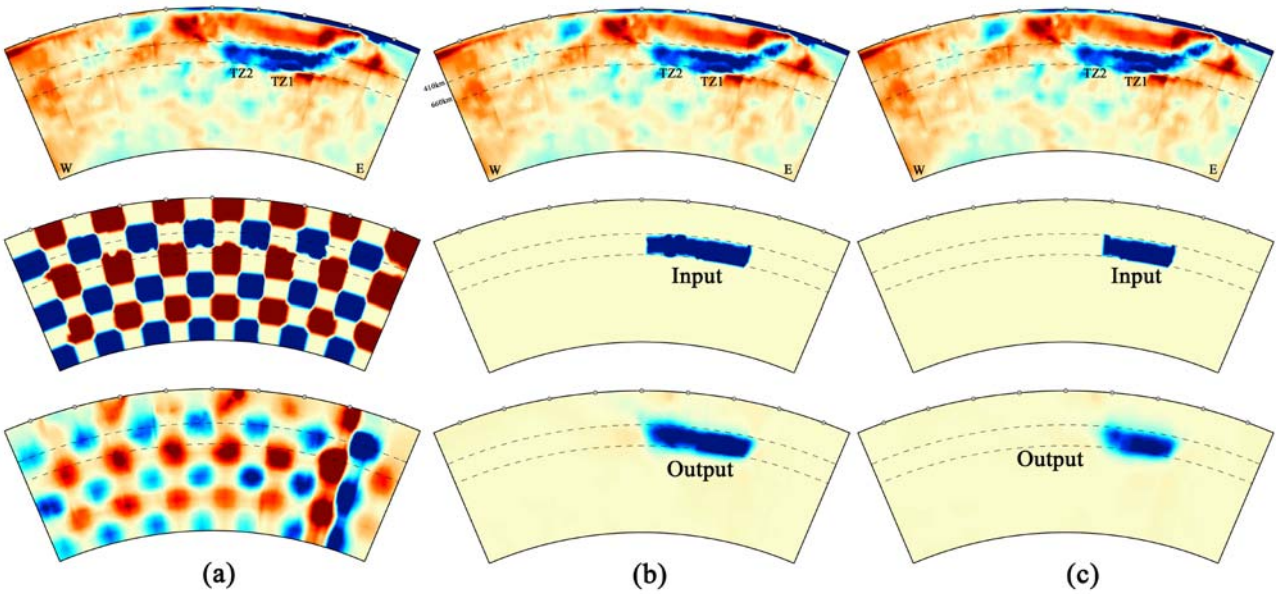

Figure 8. Tests to evaluate the resolution of the lateral extent of deflected slab (structure TZ1) in the transition zone. (a) Checkerboard resolution test; (b) target resolution test for a single, laterally contiguous structure; (c) target resolution test based on structure TZ1 as recognized in tomographic section. For each column the top plot is a tomographic section across Japan and northern China (as in Figure 6b), the middle is the input model, and the bottom is the result of inversion of data computed from the input anomaly shown in the middle plot.

Figures 4g and 6d–6g). The NE-striking structure TZ3A is located between 25°–35°N and 110°–120°E, at a depth of 500–900km (e.g., Figures 4g, 6d, and 6e). Structure TZ3B extends as far west as ~100°E; the cross sections suggest that it may connect to a shallower mantle structure west of the Sichuan basin and that at greater depths it dips westward into the lower mantle (Figure 6f).

[25] Test inversions with data computed from checkerboard and 3-D slab models suggest that the transition zone structures are well resolved. Using Figures 6b and 6e as an example, Figures 8 and 9 (left column) demonstrate that data coverage is sufficient to resolve a structure with spatial dimensions of 3° × 3° (~300 × 300 km) at most depths, including the mantle transition zone. Through the inversion of data calculated from a 3-D model with a contiguous structure in the transition zone, we explore the possibility that the separate fragments are artifacts due to uneven sampling of a large structure. Figures 8 and 9 (middle column) demonstrate that such a structure can be resolved by the data used. In another test to evaluate the lateral resolution, we performed inversions with synthetic data calculated from a 3-D model with distinct anomalies in the transition zone. Figures 8 and 9 (right column) indicate that the data can resolve separate structures, albeit with a (minor) loss of amplitude at the edges.

4. Discussion

4.1. Slab "Graveyard" in the Upper Mantle Transition Zone

[26] Along the eastern margin of Eurasia the Pacific and Philippine Sea plates are subducting beneath East Asia, creating one of the largest trench/arc/back-arc systems on Earth (Figure 1). Compared to previous tomographic studies of mantle heterogeneity beneath this complex plate boundary zone [e.g., *Van der Hilst et al.*, 1991, 1993; *Fukao et al.*, 1992, 2001; *Huang and Zhao*, 2006; *Miller et al.*, 2006], our inversions benefit from denser data coverage and yield better resolved images of subducted slabs, especially in the transition zone beneath China. Our results are consistent with results from surface-wave tomography [*Lebedev and Nolet*, 2003] but show more structural detail.

[27] One of the most pronounced deep mantle structures observed in global models [e.g., *Dziewonski and Woodhouse*, 1987; *Van der Hilst et al.*, 1997; *Bijwaard et al.*, 1998; *Castle et al.*, 2000; *Kárason and Van der Hilst*, 2001; *Grand*, 2002] is the seismically fast anomaly in the lowermost mantle beneath eastern Asia (not shown here). Its location beneath Mesozoic and early Cenozoic (convergent) plate boundaries makes it plausible that this represents a "slab graveyard" above the core mantle boundary produced by hundreds of millions of years of deep subduction (or other modes of mass transport from upper to lower mantle) along the eastern seaboard of Asia [*Ricard et al.*, 1993; *Grand et al.*, 1997; *Lithgow-Bertelloni and Richards*, 1998].

[28] In a few locations, for instance, across central Japan (Figures 6l–6n), subducting slabs in the upper mantle may still connect with, or be close to, the deep mantle structures [see, e.g., *Van der Hilst et al.*, 1997]. Overall, however, the mantle sections across Southeast Asia (Figure 6) suggest the widespread presence of subhorizontal structures between 400 and 1000 km deep beneath the Japan Sea, the East China Sea, and East China, without obvious connection to deeper structures. Following *Van der Hilst and Seno* [1993]

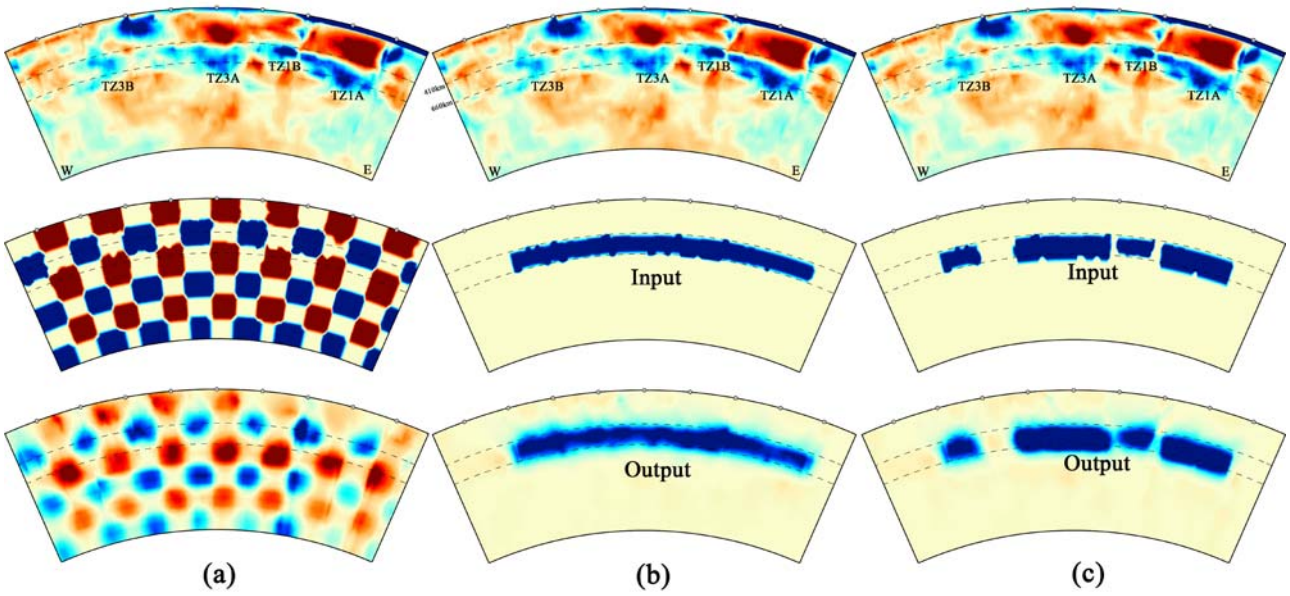

Figure 9. Tests to evaluate the resolution of separate structures in the transition zone. (a) Checkerboard resolution test; (b) target resolution test for a single, laterally contiguous structure; (c) target resolution test based on separate structures of TZ1A, TZ1B, TZ3A, and TZ3B as recognized in tomographic section. For each column the top is a tomographic section across Izu Bonin and central China (same as Figure 6e), the middle is the input model, and the bottom is the result of inversion of data computed from input anomaly shown in the middle plot.

and many later studies, we interpret these structures as fragments of subducted slabs that are stagnant in the mantle transition zone in response to (or, perhaps, as a cause of) the oceanward retreat of trench systems in the western Pacific and Indochina. It is plausible that structure TZ1 is produced by subduction of the Pacific plate at the migrating Japan and (in particular) Izu Bonin trenches and the Philippine Sea plate at the Ryukyu trench. It is unlikely, however, that these systems have produced the entire "upper mantle slab graveyard" beneath Southeast Asia as revealed in Figures 4 and 6. Given the small Cenozoic motion of Southeast Asia in the deep mantle reference frame, the position of TZ2 and TZ3 far west of modern trench systems suggests that they were not produced by recent subduction. Association with ancient subduction systems implies that stagnant slabs can reside in the transition zone for long periods of geological time.

[29] With the caveat that nonuniqueness of plate reconstructions, in particular, for this region, leaves room for different interpretations, we compare the position of the TZ structures with locations of past plate convergence and subduction. According to a reconstruction by *Honza and Fujioka* [2004], which is shown at the top in Figure 10, the Japan trench had retreated eastward over ~3000 km since the late Cretaceous (~85 Ma) and the South China trench gradually became inactive after the earliest Oligocene (~35 Ma). The map at the bottom of Figure 10 illustrates the spatial relationship between tomographically inferred transition-zone heterogeneity and the suggested locations of the South China and Japan trenches at ~85 and ~52 Ma (early Eocene). Assuming that lateral advection is small, which is reasonable in view of the results of other studies of mantle heterogeneity and plate motion [e.g., *Grand*, 1994; *Widiyantoro and Van der Hilst*, 1996; *Grand et al.*, 1997; *Van der Voo et al.*, 1999; *Replumaz et al.*, 2004; *Ren et al.*, 2007], Figure 10 indicates that structures TZ2 (in the north) and TZ3 (in the south) could have been produced by subduction along the South China and Proto-Japan trenches during the late Cretaceous to the late Eocene, that is, before Oligocene opening of the Sea of Japan, whereas TZ1 was produced by post Eocene subduction of the Philippine Sea plate along Ryukyu and the Pacific plate along the Japan and Izu-Bonin trenches.

[30] Alternatively, structures like TZ3 may have been produced by subduction (or delamination) during the Mesozoic amalgamation of cratonic units in eastern China. *Lebedev and Nolet* [2003] observed a similar structure to what we refer to as TZ3 and postulate that it might have been caused by the subduction of continental lithosphere during the Triassic-Jurassic continental collision between the South and the North China blocks. It is, indeed, likely that accretion along major suture zones was accompanied by subduction, but identifying and interpreting upper mantle structures that are possibly associated with these ancient subduction events are tenuous because (i) these structures would be old and their seismic signature weak, (ii) 3-D mantle heterogeneity beneath this region is complex and only partially resolved, and (iii) the suture zones may have moved with respect to the deeper mantle. This caveat notwithstanding, some structures shown in Figure 6 may be a "smoking gun" for ancient downwellings.

[31] For example, the deep structure of the southeastern part of the Ordos block (Figure 6i) may be a leftover from southward subduction of the lithosphere formerly attached

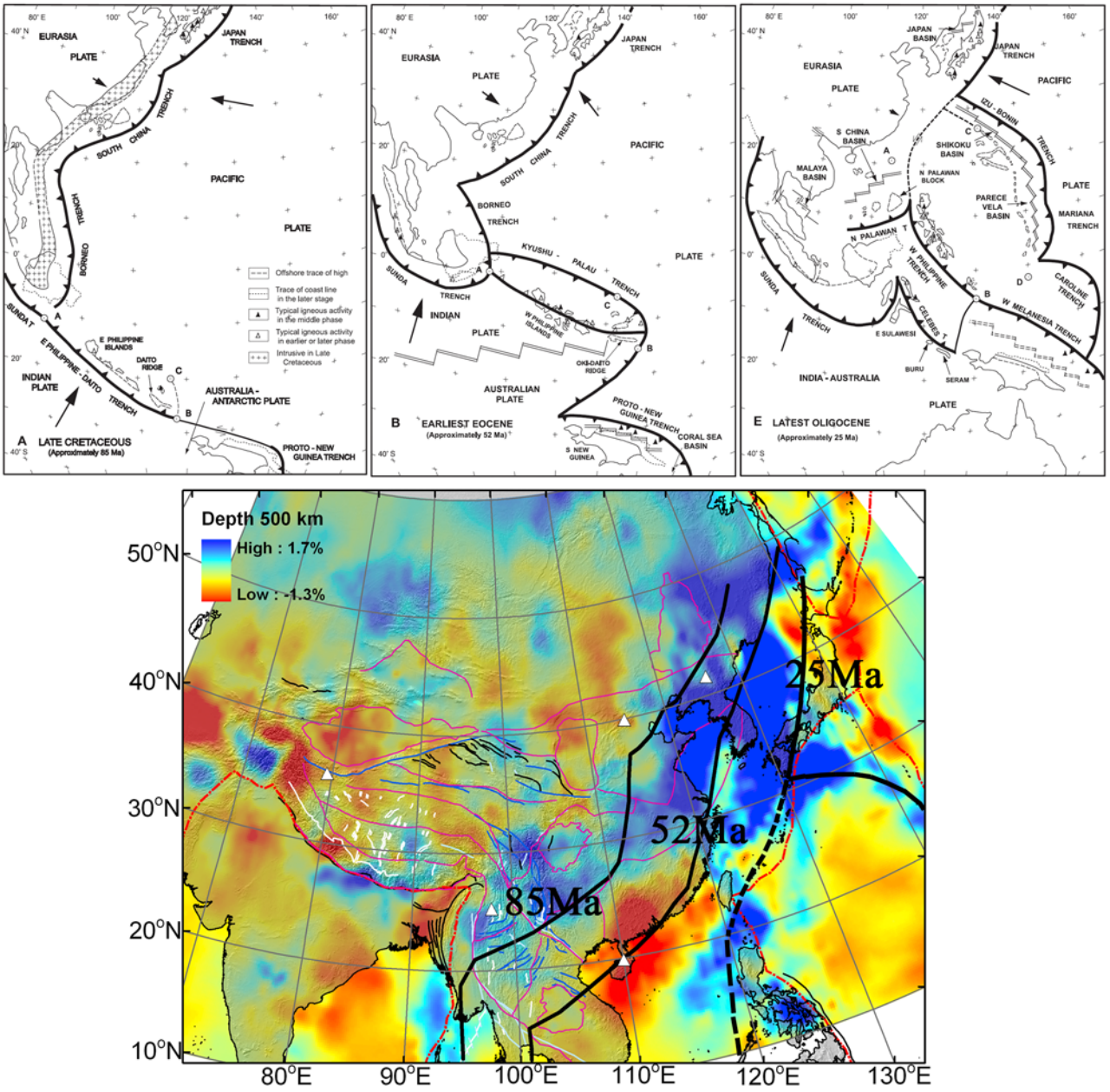

Figure 10. South China and Japan trenches in the late Cretaceous (~85 Ma) and earliest Eocene (~52 Ma) as well as the Izu Bonin trench during the latest Oligocene (~25 Ma), after the reconstruction shown in the upper plot [from *Honza and Fujioka*, 2004], superimposed on a map of tomographically inferred lateral variations in *P*-wave speed in the mantle transition zone (500 km depth) shown in the lower plot.

to the North China craton. If this process has indeed produced TZ3A, then the large (horizontal) distance between the southern tip of Ordos and TZ3A could be explained by syn- and postcollision northward displacement of the suture between the North and the South China blocks, now the Qinling-Dabie Shan, in the mantle reference frame. As another example, an intriguing SE-dipping structure in Figure 6h may represent fragments of ancient lithosphere that has somehow sunk into the deep mantle beneath the South China fold belt. This structure seems to be resolved (Figure 3), and not due to "smearing," but its 3-D structure is not known and it could be that the dip results from fortuitous alignment of separate blobs. Finally, Figures 6e–6g might suggest that TZ3B connects upward to the lithosphere of the Yangtze craton (see also Figure 4e) and downward into the lower mantle (also Figures 4e and 6f). Like the others in this paragraph, this observation is tentative, and the structural connections are not resolved, but it could relate to westward subduction of former Yangtze lithosphere (west of Sichuan Basin) during the late Cretaceous-Oligocene(?) thrusting and shortening along the

eastern margin of what is now the SE Tibetan plateau [*Tapponnier et al.*, 2001; *Burchfiel et al.*, 2008].

4.2. Anomalously Low Wave Speeds in the Upper Mantle

[32] The strongest low-wave speed anomaly is located beneath the back-arcs of the Japan and Izu Bonin subduction zones (that is, structure S1; Figures 4b–4d, 6a–6e, and 6l). In the upper 200 km or so of the mantle wedge, *P*-wave speeds are more than 2% below *ak135* reference values for the same depths (we note that the strength of the anomalies is influenced by regularization; the actual anomalies could be twice the inferred value, or more), but substantial wave-speed reductions are also observed farther away from the slabs and, in particular, at larger depths (e.g., Figures 6b, 6c, 6e, 6l, and 6n). Beneath the northern part of the Philippine Sea plate, *P*-wave propagation is very slow in the entire mantle volume contained by the upper mantle slabs of the Izu Bonin and Ryukyu subduction systems and the stagnant Izu Bonin slab in the transition zone (Figures 6d and 6e).

[33] If the low wave speed is due to dehydration of subducting slabs [e.g., *Davies and Stevenson*, 1992; *Grove et al.*, 2006], the images suggest that dehydration reactions occur over a larger depth range than commonly considered. *Revenaugh and Sipkin* [1994a, 1994b] infer from *ScS* reflectivity profiles the presence of a 50–100 km layer of partial (silicate) melt atop the 410 km discontinuity (or above deflected slabs in the transition zones) beneath eastern China and the back-arc basins of Japan and Izu Bonin. The presence of such a layer could explain parts of structure S2 (e.g., in Figures 6e, 6f, 6h, and 6i) and the deep parts of structure S1 (e.g., in Figures 6a–6c and 6l). *Bagley et al.* [2009] invoke silicate melt due to the presence of (olivine) water (up to 0.1 wt%) and temperature anomalies up to 150° C to explain the low *P*-wave speeds around a 400 km depth oceanward of the subducting Pacific plate observed by *Obayashi et al.* [2006], which are visible here in, for instance, Figures 6a–6e and 6m. The spatial extent of the extreme wave-speed drops below the northern part of the Philippine Sea plate suggests that partial melt may not be confined to the top of the transition zone but that in some situations it can also occur in shallower parts of the upper mantle. This may be a consequence of mantle flow being confined by the Ryukyu and Izu Bonin slabs on the sides and the deflected slabs below.

[34] The northern part of structure S2, in the upper mantle beneath the South China fold belt and the adjacent offshore region of the South China Sea, may be related to shallow mantle processes in the back-arc of the Ryukyu subduction system (Figures 4c, 4d, 6f, and 6i). The southern anomaly is far away from active subduction zones. It extends to at least 500 km deep beneath the South China Sea (Figures 4f and 6h) but there is no evidence of a lower mantle origin. These observations suggest that the large anomaly beneath the South China fold belt and adjacent offshore regions is related not to current back-arc processes in the mantle wedge above a subducted slab or to a "plume," but to larger-scale return flow in response to subduction farther to the (south)east, perhaps in combination with the aforementioned partial melting in the deeper parts of the upper mantle.

[35] The 3-D tomographic images indicate a connection between the deep low-wave-speed anomalies beneath the South China Sea and the South China fold belt (that is, S2) and S3, the low wave speeds in the shallow upper mantle beneath the Red River fault system (Figures 4c–4f, 6f, and 6g). This suggests that lithospheric deformation in SW China and around the Red River fault may be influenced by deeper mantle processes (much) farther to the east.

[36] The widespread slow structures in the upper mantle may be causally related to tectonic activities in East Asia. On a large scale they may have resulted in the thinning of the lithosphere under East China [*Deng et al.*, 2000], Cenozoic extension in North China [*Liu et al.*, 2001; *Zhang et al.*, 2003], and active intraplate volcanism (e.g., at the Changbai, Qiongbei, and Datong volcanoes; white triangles in Figure 4c), as discussed by *Zhao et al.* [2004]. It may also have contributed to the high heat flow and facilitated the intense deformation in Huabei, China [*Zang et al.*, 2003].

4.3. Upper Mantle Beneath and Around the Tibetan Plateau

[37] In the realm of the continental collision of India and Asia the strongest wave-speed variations occur in the top 300 km or so of the mantle. Figures 4b–4d show that *P*-wave speed in the upper mantle beneath the Tibetan plateau is several percent lower than that below the Precambrian Ordos and Sichuan basins to the east and the mountain ranges to the south (Himalaya), west (Hindu Kush, Pamir), and northwest (Tian Shan). These high-wave-speed structures are in good agreement with results from surface wave tomography [e.g., *Lebedev and Van der Hilst*, 2008], but the low wave speeds in the upper mantle beneath the Tibetan plateau inferred from *P*-wave traveltime tomography are somewhat enigmatic. Within uncertainties of both types of model (for instance, due to the differences in horizontal and vertical resolution of surface and body wave data), the low *P*-wave speed beneath much of central and northeastern parts of the plateau seems consistent with some surface wave models [e.g., *Romanowicz*, 1982; *Wu et al.*, 1997; *Friederich*, 2003; *Lebedev and Van der Hilst*, 2008] but seem at odds with the plateau-wide fast structure inferred by others [e.g., *Griot et al.*, 1998; *Shapiro et al.*, 2002; *Priestley et al.*, 2006]. On the basis of these observations, *Li et al.* [2008b] argued that the distance over which Indian lithospheric mantle underthrusts the plateau decreases from west (where it underlies the entire plateau, all the way to the Tarim basin) to east (where it seems to underlay only the Himalayan mountain belt). That is, the position of the leading edge of the Indian plate in the upper mantle runs diagonally across (and below) the crustal (lithospheric?) suture zones above it [*Li et al.*, 2008b]. This controversy, which is important for our understanding of the role of the Indian lithosphere in the evolution of the Tibetan plateau, calls for further surface- and body-wave studies with data from dense regional arrays.

[38] The realm of collision in the west (e.g., the low wave speeds beneath the central and northeastern parts of the Tibetan plateau) is separated from that of subduction in the east (i.e., the slow structures beneath the South China fold belt, S2, and the Red River fault region, S3) by the high wave speeds of the Ordos and Sichuan basins. The Sichuan basin is the Precambrian nucleus of the Yangtze craton (Figure 1). The western boundary of the largely aseismic Sichuan basin is marked by the Longmenshan fault zone,

the site of the devastating 2008 Wenchuan earthquake [*Burchfiel et al.*, 2008; *Hubbard and Shaw*, 2009]. In the north the mostly aseismic Ordos block is a major Precambrian continental nucleus of the Sino-Korean craton (Figure 1) and is surrounded by intensive intracontinental extension and high levels of seismicity. Changes in the direction of extensional stress around the Ordos block suggest that the Cenozoic rifting phase east of the Ordos block was initiated by westward subduction of the Pacific plate and that the Pliocene deformation in the southwest of the Ordos block is mainly the consequence of late-stage India-Eurasia convergence [*Zhang et al.*, 2003].

[39] At greater depths the boundary between the collision and the subduction realms may be formed by transition-zone structure TZ3B, which could have formed in late Mesozoic to early Cenozoic times by subduction along the eastern margin of what is now known as the South China fold belt (Figure 10) or, as speculated above, by subduction of the lithosphere west of the present-day Sichuan basin during the late Mesozoic-early Cenozoic stage of thrusting along the eastern margin of what is now the SE Tibetan plateau. Either scenario implies that fragments of formerly oceanic (or continental) lithosphere can reside for many tens of millions of years in the upper mantle transition zone.

5. Conclusions

[40] We present results of a tomographic inversion of *P*-wave traveltime data from a global catalog, temporary seismic arrays around the Tibetan plateau, and stations in the China provincial networks, all processed in an internally consistent way using procedures of *Engdahl et al.* [1998]. Combined, these data resolve structural heterogeneity at length scales upward of ~300 km in most of the mantle volume under the study region (roughly from 80 to 140°E, from 10 to 50°N, and to a 1000 km depth) and reveal with more clarity than before the large-scale tectonic framework of the continental India-Asia collision in the west and subduction of the oceanic lithosphere in the east. The main results pertain to the slab "graveyard" in the upper mantle transition zone, the low-velocity anomalies beneath present-day back-arc systems and the South China fold belt, and the seismically fast roots of Precambrian basins that (along, perhaps, with the transition-zone structures (fossil slabs?) below them) separate the realm of continental collision in the west (Tibet) and the Pacific realm of subduction of oceanic lithosphere along the eastern margin of Asia.

[41] Consistent with results of previous studies [*Van der Hilst et al.*, 1991, 1993; *Fukao et al.*, 1992, 2001; *Huang and Zhao*, 2006; *Miller et al.*, 2006], the data reveal transition-zone structures that are most likely due to the stagnation of subducted slabs of formerly oceanic lithosphere. This slab "graveyard" in the upper mantle transition zone is larger than previously thought, however, and the resolution of several distinct parts suggests that the structures have formed since the late Mesozoic by multiple oceanic and perhaps continental subduction systems. The deflected slab beneath the Philippine Sea plate and the eastern seaboard of Southeast Asia has been attributed to post-Eocene subduction beneath the Izu Bonin and Ryukyu arcs (*Van der Hilst and Seno* [1993] and later studies). The structures farther west (between 400 and 800 km deep beneath the Yangtze craton and South China fold belt) could have been produced earlier, for instance, in late Mesozoic to early Cenozoic times, through subduction along the SE coast of mainland China (before Oligocene-Miocene trench migration and slab roll-back and concomitant opening of marginal basins in the western Pacific) or, as proposed by *Lebedev and Nolet* [2003], during the Mesozoic amalgamation of Southeast Asia (during or after collision of the North and South China cratons). We speculate that the westernmost fragment, near 120°E, formed in the late Mesozoic by westward subduction of (oceanic? continental?) lithosphere of the South China block (west of present-day Sichuan basin) when the area now occupied by the SE Tibetan plateau was a classical fold-and-thrust belt. Whatever their origin, however, attributing the structures in the transition zone beneath the Yangtze craton to subduction implies residence times of stagnant slabs of many tens of millions of years.

[42] Low *P*-wave speeds mark the upper mantle beneath back-arcs of active subduction systems (e.g., Honshu-Nankai, Izu Bonin, and Ryukyu) and beneath the South China fold belt, the adjacent offshore of South China Sea, and the island of Hainan. The former are likely due to dehydration of the slab, and the extremely slow *P*-wave speeds beneath the northern part of the Philippine Sea plate and southern Honshu suggest that silicate melt, which may be produced by higher temperatures and water content [e.g., *Bagley et al.*, 2009], occurs throughout the upper mantle volume between the subducting slabs to the west (Ryukyu) and east (Izu Bonin) and the deflected Pacific slab. Given its distance away from active subduction and in the absence of tomographic evidence (in our images) of a deep mantle source (e.g., a "plume"), the pronounced slow anomaly beneath the South China fold belt and adjacent offshore may be due to a combination of return flow from distant subduction systems and the presence of silicate mantle deep in the upper mantle. These slow anomalies connect across the upper mantle beneath northern Indochina to strong low wave speeds in the lithospheric mantle beneath the Red River fault system in SW China.

[43] The results presented here support earlier suggestions that western Pacific subduction processes influence the thermal structure and, by implication, the deformation of the lithosphere in mainland China. Such connections have been invoked to explain extension and volcanism in NE China [e.g., *Liu et al.*, 2001; *Zhao et al.*, 2004], but we suggest that it is also the case farther south. In particular, deeper mantle processes beneath the South China Sea (including Hainan) and the South China fold belt may have influenced the thermal state and deformation of the lithosphere beneath SW China. As a corollary, deformation in these regions, including plateau formation in SE Tibet, should be viewed not just in the context of continental collision but within a larger scale framework, including mantle processes in the western Pacific realm.

[44] Consistent with the proposition by *Argand* [1924], the lateral transition between the Pacific realm (with direct influence of ongoing westward subduction of oceanic lithosphere beneath the marginal seas along the long (south) eastern seaboard of Asia) and the region more directly influenced by continental collision is formed by the remnants (or ancient nuclei) of the North and South China cratons—that is, the Ordos and Sichuan basins with ~300 km thick

continental roots—and, perhaps, fossil slabs in the upper mantle and transition zone produced by ancient collision and thrust events involving these cratons.

[45] **Acknowledgments.** We thank R. Sun, E. R. Engdahl, and E. Bergman for their fantastic work on the traveltime data from the Chinese National Network, which greatly contributed to the quality of the tomographic images shown here. We thank Paul Tapponnier, Clark Burchfiel, and Leigh Royden for many constructive discussions. This work was fund by NSF Grant 6892042 for Collaborative Research in Eastern Tibet.

References

Argand, E. (1924), La tectonique de l'Asie, *Int. Geol. Congr. Rep. Sess.*, *13*, 170–372.

Bagley, B., A. M. Courtier, and J. Revenaugh (2009), Melting in the deep upper mantle oceanward of the Honshu slab, *Phys. Earth Planet. Inter.*, *175*, 137–144, doi:10.1016/j.pepi.2009.03.007.

Barruol, G., A. Deschamps, J. Déverchère, V. V. Mordvinova, M. Ulziibat, J. Perrot, A. A. Artemiev, T. Dugarmaa, and G. H. R. Bokelmann (2008), Upper mantle flow beneath and around the Hangay Dome, Central Mongolia, *Earth Planet. Sci. Lett.*, *274*, 221–233, doi:10.1016/j.epsl.2008.07.027.

Bijwaard, H., W. Spakman, and E. R. Engdahl (1998), Closing the gap between regional and global travel time tomography, *J. Geophys. Res.*, *103*(B12), 30,055–30,078, doi:10.1029/98JB02467.

Burchfiel, B. C., L. H. Royden, R. D. Van der Hilst, B. H. Hager, Z. Chen, R. King, C. Li, J. Lü, H. Yao, and E. Kirby (2008), A geological and geophysical context for the Wenchuan earthquake of 12 May 2008, Sichuan, People's Republic of China, *Geol. Soc. Am. Today.*, *18*, doi:10.1130/GSATG18-A.1.

Castle, J. K., C. Creager, J. P. Winchester, and R. D. Van der Hilst (2000), Shear wave speeds at the base of mantle, *J. Geophys. Res.*, *105*(B9), 21,543–21,557, doi:10.1029/2000JB900193.

Chen, L., C. Cheng, and Z. Wei (2009), Seismic evidence for significant lateral variations in lithospheric thickness beneath the central and western North China Craton, *Earth Planet. Sci. Lett.*, *286*, 171–183, doi:10.1016/j.epsl.2009.06.022.

Davies, J. H., and D. J. Stevenson (1992), Physical model of source region of subduction zone volcanics, *J. Geophys. Res.*, *97*(B2), 2037–2070, doi:10.1029/91JB02571.

DeMets, C., R. G. Gordon, D. F. Argus, and S. Stein (1990), Current plate motions, *Geophys. J. Int.*, *101*, 425–478, doi:10.1111/j.1365-246X.1990.tb06579.x.

Deng, Q., X. Feng, and P. Zhang (2000), *Active Tectonics of the Chinese Tianshan Mountains*, 399 pp., Seismology Press, Beijing (in Chinese).

Dziewonski, A. M., and J. H. Woodhouse (1987), Global images of the Earth's interior, *Science*, *236*, 37–48, doi:10.1126/science.236.4797.37.

Engdahl, E. R., R. D. van der Hilst, and R. Buland (1998), Global teleseismic earthquake relocation with improved travel times and procedures for depth determination, *Bull. Seismol. Soc. Am.*, *88*, 722–743.

Friederich, W. (2003), The *S*-velocity structure of the East Asian mantle from inversion of shear and surface waveforms, *Geophys. J. Int.*, *153*, 88–102, doi:10.1046/j.1365-246X.2003.01869.x.

Fukao, Y., M. Obayashi, H. Inoue, and M. Nenbai (1992), Subduction slabs stagnant in the mantle transition zone, *J. Geophys. Res.*, *97*(B4), 4809–4822, doi:10.1029/91JB02749.

Fukao, Y., S. Widiyantoro, and M. Obayashi (2001), Stagnant slabs in the upper and lower mantle transition region, *Rev. Geophys.*, *39*(3), 291–323, doi:10.1029/1999RG000068.

Grand, S. P. (1994), Mantle shear structure beneath the Americas and surrounding oceans, *J. Geophys. Res.*, *99*(B6), 11,591–11,621, doi:10.1029/94JB00042.

Grand, S. P. (2002), Mantle shear-wave tomography and the fate of subducted slabs, *Philos. Trans. R. Soc. Eng. Sci.*, *360*(1800), 2475–2491.

Grand, S. P., R. D. van der Hilst, and S. Widiyantoro (1997), Global seismic tomography: A snapshot of convection in the earth, *Geol. Soc. Am. Today*, *7*, 1–7.

Griot, D. A., J. P. Montagner, and P. Tapponnier (1998), Phase velocity structure from Rayleigh and Love waves in Tibet and its neighboring regions, *J. Geophys. Res.*, *103*(B9), 21,215–21,232, doi:10.1029/98JB00953.

Grove, T. L., N. Chatterjee, S. W. Parman, and E. Médard (2006), The influence of H_2O on mantle wedge melting, *Earth Planet. Sci. Lett.*, *249*, 74–89, doi:10.1016/j.epsl.2006.06.043.

Hafkenscheid, E., M. J. R. Wortel, and W. Spakman (2006), Subduction history of Tethyan region derived from seismic tomography and tectonic reconstructions, *J. Geophys. Res.*, *111*(B8), B08401, doi:10.1029/2005JB003791.

Hall, R. (2002), Cenozoic geological and plate tectonic evolution of Southeast Asia and the SW Pacific: Computer-based reconstructions, model and animations, *J. Asian Earth Sci.*, *20*, 353–431, doi:10.1016/S1367-9120(01)00069-4.

Hearn, T. M., S. Wang, J. Ni, Z. Xu, Y. Yu, and X. Zhang (2004), Uppermost mantle velocities beneath China and surrounding regions, *J. Geophys. Res.*, *109*(B11), B11301, doi:10.1029/2003JB002874.

Honza, E., and K. Fujioka (2004), Formation of arcs and back-arc basins inferred from the tectonic evolution of Southeast Asia since the Late Cretaceous, *Tectonophysics*, *384*, 23–53, doi:10.1016/j.tecto.2004.02.006.

Huang, J., and D. Zhao (2006), High-resolution mantle tomography of China and surrounding regions, *J. Geophys. Res.*, *111*(B9), B09305, doi:10.1029/2005JB004066.

Huang, Z., H. Li, Y. Zheng, and Y. Peng (2009), The lithosphere of North China Craton from surface wave tomography, *Earth Planet. Sci. Lett.*, *288*, 164–173, doi:10.1016/j.epsl.2009.09.019.

Hubbard, J., and J. H. Shaw (2009), Uplift of the Longmen Shan and Tibetan plateau, and the 2008 Wenchuan (M = 7.9) earthquake, *Nature*, *458*, 194–197, doi:10.1038/nature07837.

Kárason, H. (2002), Constrains on mantle convection from seismic tomography and flow modeling, Ph.D. thesis, Massachusetts Institute of Technology.

Kárason, H., and R. D. van der Hilst (2001), Tomographic imaging of the lowermost mantle with differential times of refracted and diffracted core phases (PKP, Pdiff), *J. Geophys. Res.*, *106*(B4), 6569–6587, doi:10.1029/2000JB900380.

Kennett, B. L. N., E. R. Engdahl, and R. Buland (1995), Constrains on seismic velocities in the Earth from travel times, *Geophys. J. Int.*, *122*, 108–124, doi:10.1111/j.1365-246X.1995.tb03540.x.

Lebedev, S., and G. Nolet (2003), Upper mantle beneath Southeast Asia from *S* velocity tomography, *J. Geophys. Res.*, *108*(B1), 2048, doi:10.1029/2000JB000073.

Lebedev, S., and R. D. Van der Hilst (2008), Global upper-mantle tomography with the automated multi-mode surface and *S* waveforms, *Geophys. J. Int.*, *173*, 505–518, doi:10.1111/j.1365-246X.2008.03721.x.

Lebedev, S., T. Meier, and R. D. Van der Hilst (2006), Asthenospheric flow and origin of volcanism in the Baikal rift area, *Earth Planet. Sci. Lett.*, *249*, 415–424, doi:10.1016/j.epsl.2006.07.007.

Li, C., R. D. Van der Hilst, and M. N. Toksöz (2006), Constraining *P*-wave velocity variations in the upper mantle beneath Southeast Asia, *Phys. Earth Planet. Inter.*, *154*, 180–195, doi:10.1016/j.pepi.2005.09.008.

Li, C., R. D. Van der Hilst, E. R. Engdahl, and S. Burdick (2008a), A new global model for *P* wave speed variations in Earth's mantle, *Geochem. Geophys. Geosyst.*, *9*, Q05018, doi:10.1029/2007GC001806.

Li, C., R. D. Van der Hilst, A. S. Meltzer, and E. R. Engdahl (2008b), The subduction of Indian lithosphere beneath the Tibetan plateau and Burma, *Earth Planet. Sci. Lett.*, *274*, 157–168, doi:10.1016/j.epsl.2008.07.016.

Liang, C., X. Song, and J. Huang (2004), Tomographic inversion of Pn travel times in China, *J. Geophys. Res.*, *109*(B11), B11304, doi:10.1029/2003JB002789.

Lithgow-Bertelloni, C., and M. A. Richards (1998), The dynamics of Cenozoic and Mesozoic plate motions, *Rev. Geophys.*, *36*(1), 27–78, doi:10.1029/97RG02282.

Liu, J. Q., J. T. Han, and W. S. Fyfe (2001), Cenozoic episodic volcanism and continental rifting in northeast China and possible link to Japan Sea development as revealed from K-Ar geochronology, *Tectonophysics*, *339*, 385–401, doi:10.1016/S0040-1951(01)00132-9.

Matte, P. (1995), Southern Urals and Variscides: Comparison of their anatomies and evolutions, *Geol. Mijnbouw*, *74*, 151–166.

Miller, M. S., B. L. N. Kennett, and V. G. Toy (2006), Spatial and temporal evolution of the subducting Pacific plate structure along the western Pacific margin, *J. Geophys. Res.*, *111*(B2), B02401, doi:10.1029/2005JB003705.

Molnar, P., and P. Tapponnier (1975), Cenozoic tectonics of Asia: Effects of a continental collision, *Science*, *189*, 419–426, doi:10.1126/science.189.4201.419.

Nolet, G. (1985), Solving or resolving inadequate and noisy tomographic systems, *J. Comput. Phys.*, *61*, 463–482, doi:10.1016/0021-9991(85)90075-0.

Northrup, C. J., L. H. Royden, and B. C. Burchfiel (1995), Motion of the Pacific Plate relative to Eurasia and its potential relation to Cenozoic extension along the eastern margin of Eurasia, *Geology*, *23*, 719–722, doi:10.1130/0091-7613(1995)023<0719:MOTPPR>2.3.CO;2.

Obayashi, M., H. Sugioka, J. Yoshimitsu, and Y. Fukao (2006), High temperature anomalies oceanward of subducting slabs at the 410-km discontinuity, *Earth Planet. Sci. Lett.*, *243*, 149–158, doi:10.1016/j.epsl.2005.12.032.

Paige, C. C., and M. A. Saunders (1982), LSQR—an algorithm for sparse linear-equations and sparse least-squares, *ACM Trans. Math. Softw.*, *8*, 43–71, 195–209.

Priestley, K., E. Debayle, D. McKenzie, and S. Pilidou (2006), Upper mantle structure of eastern Asia from multimode surface waveform tomography, *J. Geophys. Res.*, *111*(B10), B10304, doi:10.1029/2005JB004082.

Ren, Y., E. Stutzmann, R. D. Van der Hilst, and J. Besse (2007), Understanding seismic heterogeneities in the lower mantle beneath the Americas from seismic tomography and plate tectonic history, *J. Geophys. Res.*, *112*(B1), B01302, doi:10.1029/2005JB004154.

Replumaz, A., H. Kárason, R. D. Van der Hilst, P. Tapponnier, and J. Besse (2004), 4-D evolution of Southeast Asia mantle structure from geological reconstructions and seismic tomography, *Earth Planet. Sci. Lett.*, *221*, 103–115, doi:10.1016/S0012-821X(04)00070-6.

Revenaugh, J., and S. A. Sipkin (1994a), Seismic evidence for silicate melt atop the 410 km mantle discontinuity, *Nature*, *369*, 474–476, doi:10.1038/369474a0.

Revenaugh, J., and S. A. Sipkin (1994b), Mantle discontinuity structure beneath China, *J. Geophys. Res.*, *99*(B11), 21,911–21,927, doi:10.1029/94JB01850.

Ricard, Y., M. A. Richards, C. Lithgow-Bertelloni, and Y. Lestunff (1993), A geodynamic model of mantle density heterogeneity, *J. Geophys. Res.*, *98*(B12), 21,895–21,909, doi:10.1029/93JB02216.

Romanowicz, B. A. (1982), Constraints on the structure of the Tibet Plateau from pure path phase velocities of Love and Rayleigh waves, *J. Geophys. Res.*, *87*(B8), 6865–6883, doi:10.1029/JB087iB08p06865.

Royden, L. H., B. C. Burchfiel, and R. D. Van der Hilst (2008), The geological evolution of the Tibetan Plateau, *Science*, *321*, 1054–1058, doi:10.1126/science.1155371.

Schellart, W. P., and G. S. Lister (2005), The role of the East Asian active margin in widespread extensional and strike-slip deformation in East Asia, *J. Geol. Soc.*, *162*, 959–972, doi:10.1144/0016-764904-112.

Schellart, W. P., M. W. Jessell, and G. S. Lister (2003), Asymmetric deformation in the back-arc region of the Kuril arc, northwest Pacific: New insights from analogue modeling, *Tectonics*, *22*(5), 1047, doi:10.1029/2002TC001473.

Shapiro, N. M., and M. H. Ritzwoller (2002), Monte-Carlo inversion for a global shear-velocity model of the crust and upper mantle, *Geophys. J. Int.*, *151*, 1–18, doi:10.1046/j.1365-246X.2002.01742.x.

Shapiro, N. M., M. Campillo, L. Stehly, and M. H. Ritzwoller (2005), High resolution surface wave tomography from ambient seismic noise, *Science*, *307*, 1615–1618, doi:10.1126/science.1108339.

Spakman, W., S. Stein, R. D. Van der Hilst, and R. Wortel (1989), Resolution experiments for NW Pacific subduction zone tomography, *Geophys. Res. Lett.*, *16*(10), 1097–1101, doi:10.1029/GL016i010p01097.

Tapponnier, P., G. Peltzer, A. Y. Le Dain, R. Armijo, and P. Cobbold (1982), Propagating extrusion tectonics in Asia: New insights from simple experiments with plasticine, *Geology*, *10*, 611–616, doi:10.1130/0091-7613(1982)10<611:PETIAN>2.0.CO;2.

Tapponnier, P., Z. Xu, F. Roger, B. Meyer, N. Arnaud, G. Wittlinger, and J. Yang (2001), Oblique stepwise rise and growth of the Tibet Plateau, *Science*, *294*, 1671–1677, doi:10.1126/science.105978.

Tatsumi, Y., S. Maruyama, and S. Nohda (1990), Mechanism of back-arc opening in the Japan Sea: Role of asthenospheric injection, *Tectonophysics*, *181*, 299–306, doi:10.1016/0040-1951(90)90023-2.

Tian, Z.-Y., P. Han, and K.-D. Xu (1992), The Mesozoic-Cenozoic East China rift system, *Tectonophysics*, *208*, 341–363, doi:10.1016/0040-1951(92)90354-9.

Van der Hilst, R. D., and T. Seno (1993), Effects of relative plate motion on the deep structure and penetration depth of slabs below the Izu-Bonin and Mariana island arcs, *Earth Planet. Sci. Lett.*, *120*, 395–407, doi:10.1016/0012-821X(93)90253-6.

Van der Hilst, R. D., E. R. Engdahl, W. Spakman, and G. Nolet (1991), Tomographic imaging of subducted lithosphere below northwest Pacific island arcs, *Nature*, *353*, 37–43, doi:10.1038/353037a0.

Van der Hilst, R. D., E. R. Engdahl, and W. Spakman (1993), Tomographic inversion of *P* and *pP* data for aspherical mantle structure below the northwest Pacific region, *Geophys. J. Int.*, *115*, 264–302, doi:10.1111/j.1365-246X.1993.tb05603.x.

Van der Hilst, R. D., S. Widiyantoro, and E. R. Engdahl (1997), Evidence for deep mantle circulation from global tomography, *Nature*, *386*, 578–584, doi:10.1038/386578a0.

Van der Voo, R., W. Spakman, and H. Bijwaard (1999), Tethyan subducted slabs under India, *Earth Planet. Sci. Lett.*, *171*, 7–20, doi:10.1016/S0012-821X(99)00131-4.

Widiyantoro, S., and R. D. Van der Hilst (1996), Structure and evolution of subducted lithosphere beneath the Sunda arc, Indonesia, *Science*, *271*, 1566–1570, doi:10.1126/science.271.5255.1566.

Wu, F. T., A. L. Levshin, and V. M. Kozhevnikov (1997), Rayleigh wave group velocity tomography of Siberia, China and the vicinity, *Pure Appl. Geophys.*, *149*, 447–473, doi:10.1007/s000240050035.

Yao, H., R. D. van der Hilst, and M. V. de Hoop (2006), Surface-wave array tomography in SE Tibet from ambient seismic noise and two station analysis: I. Phase velocity maps, *Geophys. J. Int.*, *166*, 732–744, doi:10.1111/j.1365-246X.2006.03028.x.

Yao, H., C. Beghein, and R. D. Van der Hilst (2008), Surface-wave array tomography in SE Tibet from ambient seismic noise and two-station analysis: II. Crustal and upper mantle structure, *Geophys. J. Int.*, *173*, 205–219, doi:10.1111/j.1365-246X.2007.03696.x.

Yin, A. (2000), Mode of Cenozoic east-west extension in Tibet suggesting a common origin of rifts in Asia during the Indo-Asian collision, *J. Geophys. Res.*, *105*(B9), 21,745–21,760, doi:10.1029/2000JB900168.

Zang, S., C. Li, J. Ning, and R. Wei (2003), A preliminary model for 3-D rheological structure of the lithosphere in North China, *Sci. China*, *D46*(5), 461–473.

Zhang, Y., Y. Ma, N. Yang, W. Shi, and S. Dong (2003), Cenozoic extensional stress evolution in North China, *J. Geodyn.*, *36*, 591–613, doi:10.1016/j.jog.2003.08.001.

Zhao, D. P., J. S. Lei, and R. Y. Tang (2004), Origin of the Changbai intraplate volcanism in Northeast China: Evidence from seismic tomography, *Chin. Sci. Bul.*, *49*(1), 401–1408.

Zhou, H. W., and R. W. Clayton (1990), *P*- and *S*-wave travel time inversions for subducting slab under the island arcs of the Northwest Pacific, *J. Geophys. Res.*, *95*(B5), 6829–6851, doi:10.1029/JB095iB05p06829.

Zonenshain, L. P., V. G. Korinevskiy, V. G. Kazmin, V. V. Matveenkov, and V. Khain (1984), Plate tectonic model of the South Urals, *Tectonophysics*, *109*, 95–135, doi:10.1016/0040-1951(84)90173-2.

C. Li, Geoscience Technology, Hess Corporation, 500 Dallas Street, Houston, TX 77002, USA. (changli007@gmail.com)

R. D. van der Hilst, Department of Earth, Atmospheric, and Planetary Sciences, Massachusetts Institute of Technology, 77 Massachusetts Avenue, Cambridge, MA 02139, USA.